Advanced BDTN Inlet Design for Superior STOL Performance in Military Aircraft: A Computational Fluid Dynamics Investigation

A report submitted in partial fulfillment of the requirements for the degree of

Bachelor of Technology

in

Aerospace Engineering

by

Syesha Kumar **Aniket Kumar Singh**

R290221067 **R290221011**

Riya Sahu **Jasmeet Singh Nagpal**

R290221086 **R290221031**

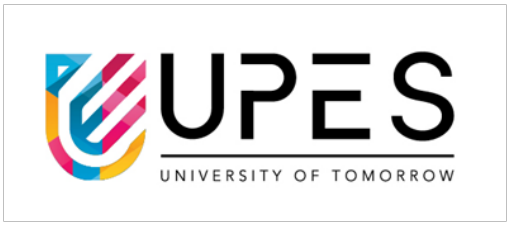

DEPARTMENT OF AEROSPACE ENGINEERING
SCHOOL OF ADVANCED ENGINEERING
UNIVERSITY OF PETROLEUM AND ENERGY STUDIES
Dehradun - 248007

May, 2025

Department of Aerospace Engineering
Dehradun, Uttarakhand-248007

CERTIFICATE

It is certified that the work contained in the project titled "***Advanced BDTN Inlet Design for Superior STOL Performance in Military Aircraft: A Computational Fluid Dynamics Investigation***" by following students has been carried out under our supervision. The content of this report is original and has not been submitted elsewhere for the award of any academic or professional degree.

	Student Name	***Roll Number***	***Signature***
1.	Syesha Kumar	R290221067	
2.	Aniket Kumar Singh	R290221011	
3.	Riya Sahu	R290221086	
4.	Jasmeet Singh Nagpal	R290221031	

Mr. Ramesh Kumar
Project Supervisor
Mechanical Cluster
SOAE
Dehradun, Uttarakhand
India - 248007

Dr. Harshit Shukla
Project Co-supervisor
Mechanical Cluster
SOAE
Dehradun, Uttarakhand
India - 248007

Dr. Ram Kunwer
Activity Coordinator
Mechanical Cluster
SOAE
Dehradun, Uttarakhand
India - 248007

ACKNOWLEDGEMENT

We take this opportunity to express our sincere thanks to our supervisors Mr. Ramesh Kumar and Dr. Harshit Shukla for their guidance and support. We would also like to express our gratitude towards them for showing confidence in the team. It was a privilege to have a great experience working with them in a cordial environment.

We are very grateful to the University of Petroleum and Energy Studies for providing us the opportunity of pursuing the Bachelors of Technology in Aerospace in a peaceful environment with ample resources. We are also thankful to the institute for providing us with the opportunity to present our work at several national and international conferences in future. We are very grateful to Dr. Kumar Gaurav for his cordial support in utilizing the Computational Fluid Dynamic Research Laboratory to conduct the necessary analysis.

The author is also thankful to the team Aniket Kumar Singh, Riya Sahu, Jasmeet Singh Nagpal and friend Divyank Aggarwal, office staffs Shree Om sir, and others, for their warm support.

In the end, we would like to acknowledge our parents, family members. Without their support, this work would not have been possible.

Syesha Kumar

Aniket Kumar Singh

Riya Sahu

Jasmeet Singh Nagpal

ABSTRACT

This study numerically investigates the advanced exhaust designs of the bypass dual throat nozzle (BDTN), to achieve desirable performance for the operation of the short take-off and landing (STOL) in military aircraft. The design consists of a classic BDTN part with a curved conduit that injects the flow back into the primary flow, at an injector or bypass angle (α). This detailed flow analysis has been performed to investigate various flow performance parameters such as thrust deflection angles (δ), thrust coefficient (C_t), lift coefficient(C_{fy}) and thrust losses at different injection angles, inlet diameters of the curved conduit and nozzle pressure ratio (NPR) using computational fluid dynamics (CFD) - ANSYS 2024 R1. The investigated performance comparison is shown graphically using Origin Pro and analytically using EXCEL. The analysis for the STOL operating condition of the engine exhaust was conducted for varying bypass conduit width and NPR. At engine operating condition of 4 NPR, selected as the STOL condition, the further investigation of the engine performance was conducted for different injection angles in range of 35° to 75°, to maintain the counter flow interaction of the primary and secondary flow. At the bypass injection angle of 70°, the resulting maximum deflection angle, δ of 24° was achieved with minimal thrust losses of around 1.6% and production of thrust vertical lift or C_{fy} of 0.3 at STOL mode phase of the engine. This was carried out by extensive computational modeling, using RANS realizable k-ϵ model for the analysis of exhaust flow behavior. The validation of the flow behavior was conducted for the pressure distribution especially at the cavitation region located in the divergent section of BDTN configuration. This thrust deflection is efficiently controllable through valves, the performance of which has also been predicted under different nozzle pressure ratio (NPR). The efficient removal of the mechanical components from the engine gave a wide margin in the weight reduction from the conventional nozzle, with improved super maneuverability operation of the military aircraft. The optimized design for the exhaust BDTN system showed more than satisfactory short take off and landing performance, with enhanced controlled maneuverability of the flow. This system offers future research scope for considering BDTN, along with integrated design study on controlled flow mechanisms in the BDTN configuration of the exhaust system to achieve the STOL operation efficiently.

Keywords

BDTN Inlet Design CFD, Military STOL Aircraft, Design Optimization, Performance Enhancement, Turbulence Modeling Realizable $k-\epsilon$, Flow Validation, Nozzle STOL Operating Condition, Thrust Vectoring, Lift Enhancement, Secondary Flow Inlet Behavior.

Table of Contents

List of Symbols & Abbreviations

ϵ	Dissipation rate
α, β_1	Injection Angle
δ	Thrust deflection angle
3BSN	Three bearing swivel nozzle
α_1	First convergence angle
β	Injection Angle
δ_h	Horizontal thrust deflection
δ_v	Vertical thrust deflection
γ	Specific heat ratio
$\overline{m}_{in}$	Mass flow rate
ρ	Density of the flow
τ_{wall}	Shear Wall Stress
θ_1	Divergence angle
θ_2	Second convergence angle
A_2	Nozzle area at 2^{nd} throat
A_x	Projected area along horizontal axis
A_y	Projected area along vertical axis
A_{in}	Nozzle inlet area
C_p	Coefficient of Pressure
C_t	Thrust coefficient
C_{fy}	Thrust lift coefficient

$C_{l_{max}}$ Overall lift coefficient of aircraft

$C_{l_{wing}}$ Lift coefficient of wing

E_r Expansion Ratio

F_x Force in axial direction

F_y Force in radial direction

F_{comp} Resultant computational force

F_{ideal} Isentropic ideal force

F_{wall-x} Axial force component on wall

F_{wall-y} Normal force component on wall

H_2 Secondary throat height

H_{in} Primary inlet height

k Turbulent Kinetic energy

L_{cav} Cavity length

M_a Mach number

P_b Ambient Pressure

P_o Total Pressure

P_{amb} Total Ambient pressure

R Gas constant

T Total Temperature

v_x Velocity in axial or x-direction

v_y Velocity in normal or y-direction

V_{in} Inlet velocity

W_b Bypass conduit inlet width

H_f/H_{in} Far field Height ratio

L_f/L_{cav} Far field length ratio

AMR Adaptive Mesh Refinement

AUTOCAD Automatic Computer Aided Design

BDTN Bypass Dual Throat Nozzle

CD Convergent Divergent

CFD Computational Fluid Dynamics

CFI Counter-Flow Injection

DES Detached eddy simulation

DNS Direct Numerical Solution

DTN Dual Throat Nozzle

FTVC Fluid Thrust Vector Control

FVNM Finite Volume numerical method

LES Large Eddies Simulation

MATLAB Matrix Laboratory

MTVC Mechanical Thrust Vector Control

NPR Nozzle Pressure ratio

P Pressure

RANS Reynolds Average Navier Stokes

RCS Radar Cross-section

RFDSS Roe's Flux difference splitting scheme

S/VTOL Short or Vertical take off and landing

SAI Secondary air injection

SGI Secondary Gas Injection

SPR Secondary pressure ratio

STOL Short take off and landing

STOVL Short take off and vertical landing

SVC Shock Vector Control

TVC or TC Thrust Vectoring Control

VTOL Vertical Take-off and landing

List of Figures

List of Tables

Chapter 1

Introduction

It is vital for any military vehicle to have a significant strategic and tactical advantage that allows them to operate in a wider range of environments, a faster response time that improves survival and provides necessary support. In combat scenarios, STOL aircraft can not only operate from shorter, dispersed, and potentially damaged runways, but also on unimproved surfaces such as roads or fields, especially in disaster-prone areas, thus improving life and operational flexibility in different military operations. This allows the STOL aircraft to efficiently deliver essential supplies and deploy troops for support, personnel, and even medical aid. From delivering essential aid in disaster-stricken regions where the traditional airport infrastructure is compromised to projecting power in remote and contested territories, STOL technology directly addresses the evolving demands of global security and rapid response. Furthermore, advancements in efficient thrust vectoring systems, such as the bypass dual throat nozzle (BDTN), hold the potential to not only improve STOL performance but also to enhance aircraft maneuverability and overall mission effectiveness, impacting the design and operational doctrines of military aviation across the globe.

The Lockheed Martin F-35 B Lightning II's is currently the most prominent modern fighter aircraft with Short Take-off and Vertical Landing (STOVL) capability which makes use of the swivel nozzle technology, shown in figure 1.1 below, to achieve thrust vector control, while Harrier's Rolls-Royce Pegasus engine remains the iconic example of STOVL making use of the rotating nozzles. The Bell Boeing V-22 Osprey, although not a fixed wing fighter, is also considered a STOL aircraft with its tilt rotor technology. The above mentioned are the only aircraft that achieve the STOL operations upon optimization of exhaust engine design. Significant research efforts have been dedicated to exploring various methods for achieving superior STOL performance, with a notable focus on exhaust nozzle design and thrust vectoring techniques. Mechanical thrust vectoring systems (mentioned above), while proven, often introduce additional weight and other complexities.

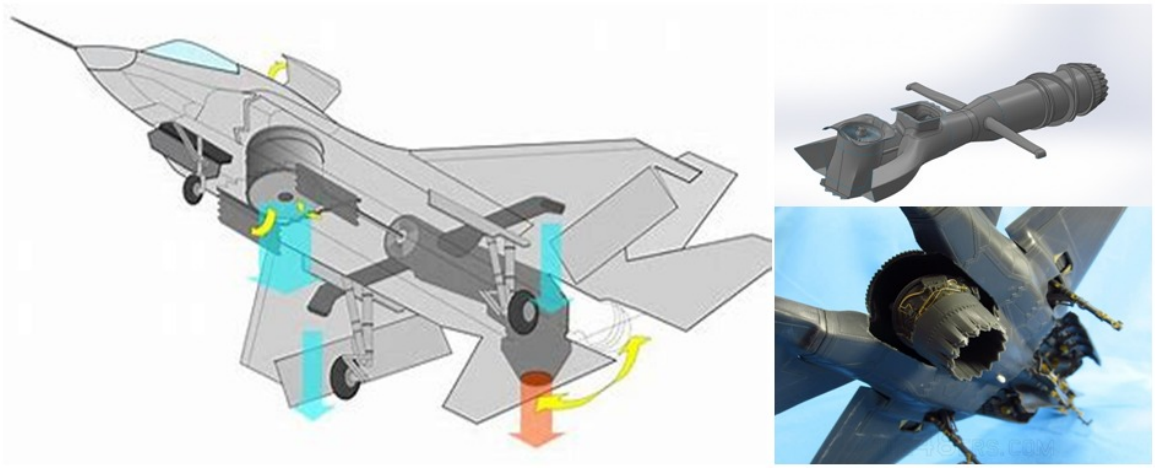

Figure 1.1: Mechanical thrust vector using Swivel nozzle technique in F 35 B[1,2,3]

Consequently, fluidic thrust vectoring methods, including those employing secondary gas injection and bypass concepts, have garnered increasing attention, for their potential to offer lighter and more integrated solutions. While the fundamental principle of BDTN have been investigated, the specific design and optimization of the inlet geometry to maximize thrust vectoring efficiency and minimize performance losses for advanced military aircraft remain areas, thus requiring in-depth exploration Previous studies have laid the groundwork by examining the general flow characteristics and performance potential of BDTN configurations, but a comprehensive computational investigation focusing on the nuanced design of the inlet for superior STOL performance has yet to be fully realized. As a result, fighter aircraft with integrated functions and a good balance of convenience and performance are steadily growing in demand within this contemporary defense sector.

1.1 Motivation

This stems from the desire to enhance operational capabilities and overcome limitations associated with traditional fixed-wing aircraft. The enhanced STOL performance offers more efficient fluidic thrust vectoring techniques such as BDTN, which aims at reducing thrust losses and is less complex compared to mechanical systems. This leads to greater vertical lifting and control during STOL operations. With improved control at low speeds, thrust vectoring provides enhanced maneuverability, which is crucial for safe and effective STOL flights. This also allows for expanding the operational flexibility with access to austere environments, increasing deployment option with increase in payload and range which extends their mission effectiveness. More scope for carrier operations as can be observed in figure 1.2, especially for naval aviation, which operates from smaller aircraft carriers without the need for catapults and arresting gears, allows the reach of naval air power to be expanded. This technological advancement brought about by novel engineering solutions pushes the

boundaries of propulsion and aerodynamic engineering, leading to innovative solutions for complex flight challenges. Research in the integration of future aircraft design can inform the design of next-generation military aircraft, potentially leading to more versatile and adaptable platforms. This investigation of BDTN provides a valuable comparison against other STOL methods such as lift-fans used in F-35 B or tilt rotors in V-22 Osprey, to determine the most effective solution for specific aircraft types and mission requirements.

(a) Dirt strip[4] **(b)** Aircraft carrier[5]

Figure 1.2: Types of inadequate runways

1.2 Objectives

This research has been conducted on the basis of the above-mentioned desired requirements to optimize the BDTN injection design that achieves enhanced STOL performance for the military fighter jets. Evaluation of performance parameters of the same aims to study detailed analysis of flow characteristics, vectoring angles, thrust coefficients, and percentage losses for various BDTN configurations. Thus, opening doors for exploration for design variations parameters like bypass angle (α) and optimal conduit width to identify optimal design configurations.The project has therefore been partitioned into two segments to achieve the best possible outcome of this project. Thus, this study has considered the following objectives for the entire research investigation:

1. OPTIMIZING NOZZLE DESIGN FOR STOL APPLICATION
2. PERFORMANCE ESTIMATION and VALIDATION

This report presents a detailed computational fluid dynamics (CFD) investigation into a BDTN inlet design aimed at achieving the desirable STOL performance in military aircraft. Through meticulous numerical simulation, various innovative inlet geometries are analyzed to assess their impact on the key performance parameters, including thrust coefficient (C_t), lift coefficient (C_{fy}), derived from thrust vectoring and thrust deflection angle (δ). The study focuses on identifying an optimized inlet configuration that enhances the interaction between the primary and bypass flows, thereby

maximizing the vertical thrust component crucial for short take-offs while minimizing associated performance penalties, at optimal engine STOL condition. The observation of these simulations provide valuable insights into complex flow physics within the BDTN and offer a pathway towards the development of more effective STOL-enabling exhaust nozzle designs. This research seeks to quantify how BDTN-enabled thrust vectoring can enhance fighter jet maneuverability and control authority at low speeds, which are critical phases of STOL operations. The report provides a comprehensive review of the relevant literature on STOL technology, thrust vectoring techniques and existing BDTN research, following extensive computational methodology employed for the parametric investigation, including governing equations, turbulence model (detailed in Appendix A), mesh generation strategy and boundary conditions. The findings and the representation of the analysis obtained from the CFD simulations has also been discussed, following the key observations, drawing conclusion regarding the effectiveness of the proposed inlet designs, and outlines potential avenues for future work and development in various critical areas.

Chapter 2

Literature Review

Thrust vectoring (TV) is a crucial technology to enhance maneuverability and STOL capabilities of the military aircraft engine exhaust system. This section briefly examines the results of the research conducted on various TV techniques, such as mechanical and fluidic thrust vectors, to enhance the STOL.

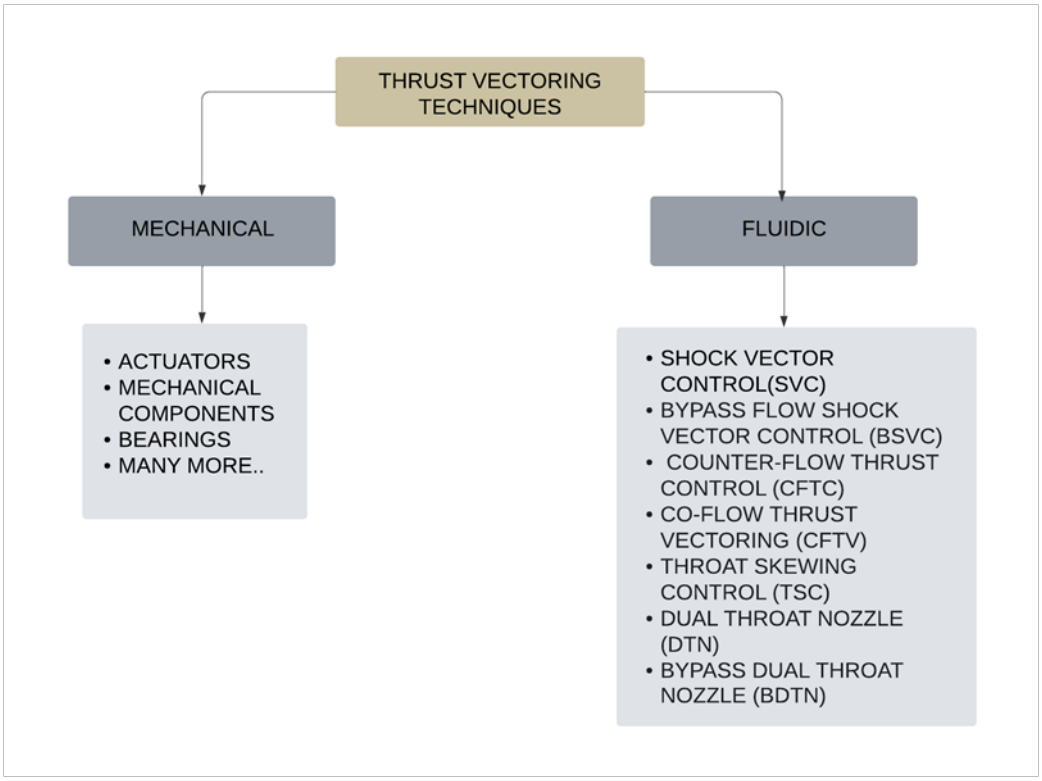

Figure 2.1: Characteristics of thrust vector control methods

Mechanical thrust control (TC) involves physically deflecting the exhaust plume using movable nozzle components. Common techniques include:

- **Swivel Nozzles:** The entire nozzle or sections of it pivot to reduce thrust. This method, famously used in the Harrier [6] in 1967, can achieve large vectoring angles (up to 90 ° for vertical lift), but often results in significant weight

and complexity. The thrust coefficient C_t losses significantly low during non-vectored flight but may increase with larger deflection angles due to non-ideal flow expansion.

- **Rotating Vanes/Paddles:** When inserted into the exhausted stream, the paddles deflect the flow, which offers a faster response time compared to swivel nozzles. This typically achieves smaller vectoring angles and can introduce substantial C_t losses due to flow blockage and increases the surface area.
- **Flexible Nozzles:** This makes use of flexible materials to change the exit area and the direction of the exhaust. Although potentially lighter, they often face challenges in terms of durability and achieving large vectoring angles with minimal C_t losses.

Although mechanical thrust vector control (MTVC) achieves a high vector angle (δ), especially with swivel nozzles and tilt rotors, it is a relatively mature and well-understood technology. With an increase in weight and complexity due to actuators, linkages, and moving parts, offer potential for higher maintenance requirements and may also introduce significant aerodynamic drag[7] and increases radar cross-section (RCS) in some designs, as is evident from Figure 2.3. Thus, allowing researchers to explore fluidic thrust vector control techniques (FTVC) to overcome the disadvantages offered by the MTVC techniques.

Classification	**Mechanism**	**Advantages**	**Disadvantages**
Mechanical	Vanes/flaps, Gimbal mounts	Proven technology, precise control	Complex design, adds weight
Fluidic	Internal airflow manipulation	Simpler design, potentially faster response	potential for lower control precision

Table 2.1: Comparison between MTVC and FTVC

Fluidic TV manipulates the exhaust flow using the injection of secondary fluid or geometric modifications within the nozzle, eliminating the need to move mechanical parts in the primary exhaust stream. Some of the FTVC techniques include:

- **Secondary Gas Injection (SGI):** Injecting a secondary fluid (typically bleed air from the engine) into the primary exhaust stream near the nozzle exit can create shock waves or pressure gradients that deflect the main jet as shown in Figure 2.2 . Studies have shown that SGI can achieve vectoring angles up to

15-20 ° with relatively low C_t losses of about 1 to 3% at lower injection rates[8] . However, higher injection rates for larger angles can lead to significant thrust penalties.

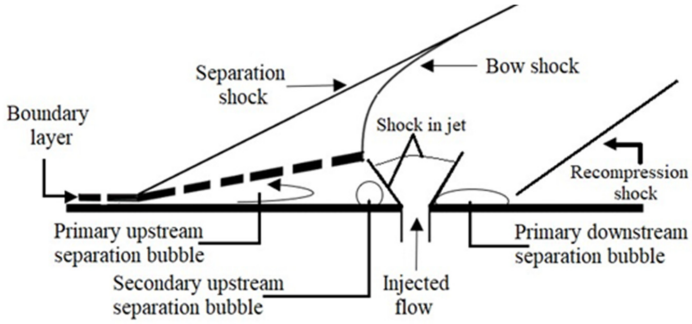

Figure 2.2: Schematic Flow Behavior upon SGI[9]

- **Counter-Flow Injection (CFI):** It involves injecting secondary air upstream and counter to the primary flow can also induce thrust vectoring. A research study[10] indicated that CFI can achieve vector angles comparable to SGI but may have varied effects on flow instability and mixing.

- **Shock-Vectoring Control (SVC):** By utilizing tactically placed tabs or wedges within the divergent section of a convergent-divergent (CD) nozzle, can help generate oblique shock waves that deflect the exhaust flow. SVC offers a simple mechanical implementation compared to full mechanical vectoring, thus achieving δ (vectoring angles) of around 10 - 15 ° with reported C_t losses of less than 1%[11].

- **Bypass Dual Throat Nozzle (BDTN):** This involves a bypass duct or conduit that allows secondary or compressed air to interact with the primary exhaust within a dual throat nozzle. Upon gaining control of the bypass flow rate, injection geometry, and pressure distribution, the direction of the primary jet can be altered. The numerical investigation demonstrated the potential of BDTN to achieve significant δ, up to 30 °, and potentially more with optimized designs with promisingly low C_t losses, generally in the range of 1 to 2%[12,13] in some configurations.

FTVC offers reduced inertia, allowing for potentially faster vector response rates that require fewer moving parts in the primary exhaust system, thus reducing maintenance[14]. It can be integrated more seamlessly within certain nozzle designs, potentially reducing drag. This research focuses on potentially lower weight and complexity compared to the mechanical system offered by the FTVC technique BDTN which shows marginal promise for larger δ.

Evaluation Criteria	Diagram	Design	Impact on System	Implementation	TV angle	Thrust Coefficient	Thrust efficiency	Thrust losses	Negative Consequences	Potential Problem
SVC	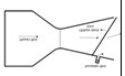	Secondary flow injection in the supersonic region	Reduces the maximum resultant thrust	Readily integrated into existing systems	Large	Lower	Higher	Higher	Large thrust losses	High differential pressure losses. In fully expanded conditions, the oblique shock wave is less effective in deflecting the primary flow
BSVC		A bypass flow injection in the divergent section	No secondary injection requirement	Readily integrated into existing systems	Small	Higher	Lower	Higher	Complex flow field	Shock waves induced at a higher SPR are insufficient for vector operation because they interact with the opposite wall at a higher bypass injection angle
CFC	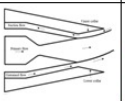	Secondary flow penetrated in the opposite direction of primary flow	No moveable parts for flow vectoring	Critical design Required for optimum performance	Large	Higher	Higher	Higher	Hysteresis, suction source and integration problems	Connection of the main jet to the suction collar
Co-Flow	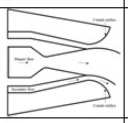	Secondary flow penetrated along with the primary flow	Minimal momentum loss	Critical design Required for optimum performance	Small	Lower	Lower	Lower	Limitation on TV angle	Connection of the main jet to the suction collar
TSC		Asymmetrical injection in the throat	No shock losses	Readily integrated into existing systems	Small	Higher	Higher	Lower	Low performance	Vectoring and jet area control are possible simultaneously, but it can be difficult to separate them
DTN		Secondary flow is injected in the upstream minimum area	Enhanced performance due to the cavity regions	Readily integrated into existing systems	Large	Higher	Higher	Lower	High-pressure secondary injection	TV operation adversely affects discharge coefficient
BDTN	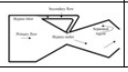	Bypass is introduced at the upstream throat	No thrust losses	Readily integrated into existing systems	Large	Higher	Higher	Lower	No negative consequences predicted until now	So far, no potential problems were listed in the literature

Table 2.2: Comparison of different FTVC Techniques[15]

Bypass dual throat nozzle is a modification of the dual throat nozzle (DTN), designed to improve thrust vectoring performance and also introducing the result thrust losses from bleeding air from the engine compressor or fan[16] or the exhaust flow by additional chemical mixing[17] of the flow at the first throat of the design configuration. This approach aims to achieve effective thrust vectoring while mitigating some of the drawbacks of other methods as discussed in table 2.2.

2.1 Research Gap

In 1989, Bell and Boeing developed the tilt rotor, or 'Prop-rotors' which is used in the V-22 Osprey, which had the ability to hover and fly like a drone and the usual characteristics of a normal fighter carrier. The multifunctional design resulted in it's performance in both vertical flight mode and cruise mode to be affected with failure of one engine, hydraulic instabilities, and flight control systems that produced many fatal crashes, while switching to different flight modes during flight.

Moreover, the design of the V-22 Osprey tilt-rotor, a crucial cargo combat aircraft, that indulges in deploying troops, weaponry, and machines. During the hovering and transition phases of the tilt rotor, the vortex rings formed from the propeller wash and the exhaust from the nozzle resulted in increased time during transition and failure of

the engine at higher flow speeds[7]. In addition, it is expensive to maintain and has a high weight of mechanical components, especially on the wing tips, leading researchers to opt for some alternatives and improve the performance of such aircraft in combat.

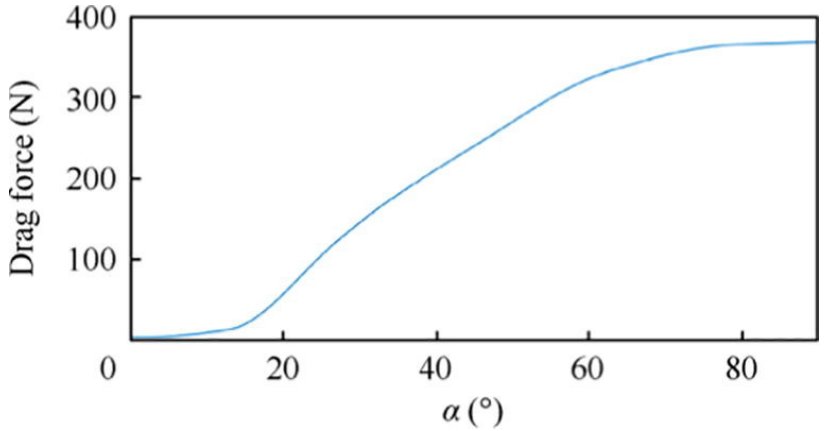

Figure 2.3: Dynamic effects on Drag Force during Transition in Tilt-rotor[7]

The year 1971 introduced two-lift jet nozzles for a Russian fighter jet Yak-38 Forger that incorporated vertical take-off and landing (VTOL) specifications[18]. This type of nozzle had a simplified design compared to the tilt rotor, with a reduced weight and increased payload capacity, and improved hover stability and control. However, there was a reduction in the forward speed due to the deduction of the thrust from the lift jet, the complexity of the control and coordination of the lift jet, and there was a high fuel consumption during the VTOL phase.

The recent improvement in the mechanical components of the engine's exhaust system for S/VTOL was in 2015, when the Lockheed Martin F-35 B was introduced in the defense industry. The main turbo engine is the same as the conventional take-off and landing configuration, while a shaft-driven lift fan and a three-bearing swivel nozzle (3BSN) were installed [19]. The rotational angle included 0-95 °. Although this innovative design opened different propulsion areas for further conceptual studies and effects, the design of the mechanical structure and bearing connection is complex to understand due to the demand for complicated design processes in the actuation and control system.

From the historical development of FTVC as shown in Figure 2.4, BDTN is an emerging technology that aims to improve STOL performance by providing efficient thrust vectoring and potentially reducing C_t losses compared to traditional methods. The conceptual design of the research[20,21] shows that BDTN is achieved by adding the secondary throat to the primary flow. The investigation[14] of the design typically features a primary exhaust stream from the engine core and a percentage of the conduit stream that is extracted from the former exhaust flow or from a secondary bypass

stream, often from the compressor section of a turbojet engine.

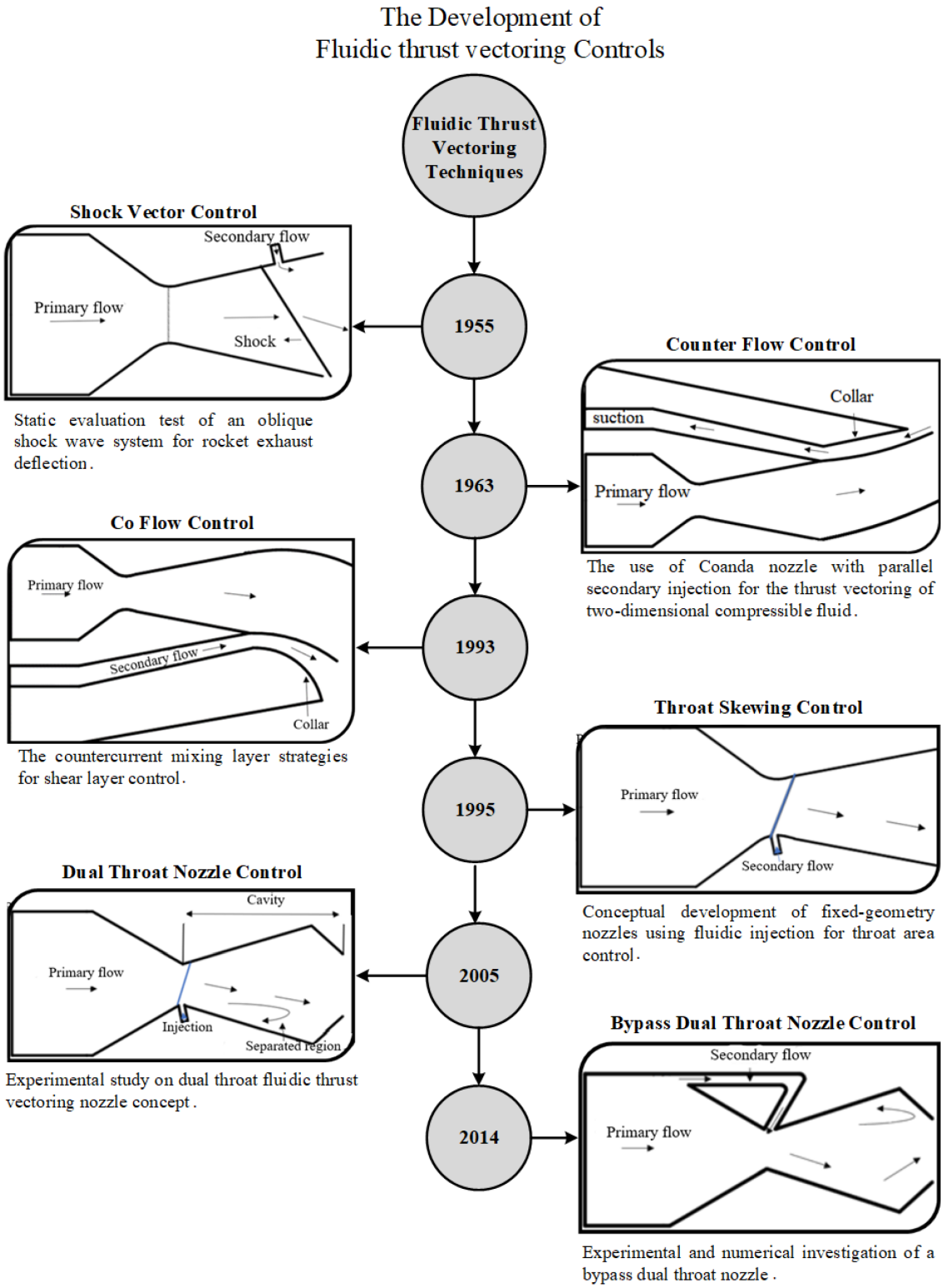

Figure 2.4: Historical flowchart of FTVC[22]

The key to TV lies in the controlled mixing and deflection of these flows, often facilitated by a cavity or expansion chamber located downstream of the throats[12] as

shown in Figure 2.6. The NPR significantly influence the flow characteristics within the nozzle, including, the behavior of the shock waves, the interaction between the primary and secondary bleed flow and ultimately, thrust vectoring angle and efficiency. Research clearly indicates that the performance of BDTNs varies considerably with changes in NPR, and optimizing the design for a specific NPR range is crucial[16,23,24]. Controlling or modulating the secondary mass flow rate is a key aspect of BDTN operation. Studies have investigated how varying the amount of secondary air injected into the nozzle affects the thrust vectoring angle, thrust production and overall efficiency of the system[24]. Precise control of the secondary mass flow rate[25] is essential for achieving accurate and responsive TV. To achieve better flow uniformity, studies[26,27] have used CFD to analyze the flow characteristics and performance of axis symmetric divergent BDTN designs. The single plane thrust vectoring, typically provides deflection in only one axis, investigates different multiplane TV nozzle designs, and comparing their effectiveness in terms of vectoring angles, thrust losses, control authority and more[28]. The core concept of simultaneously controlling the thrust vector in two or more axes, namely pitch and yaw, enables more complex flight maneuvers and control capabilities[29].

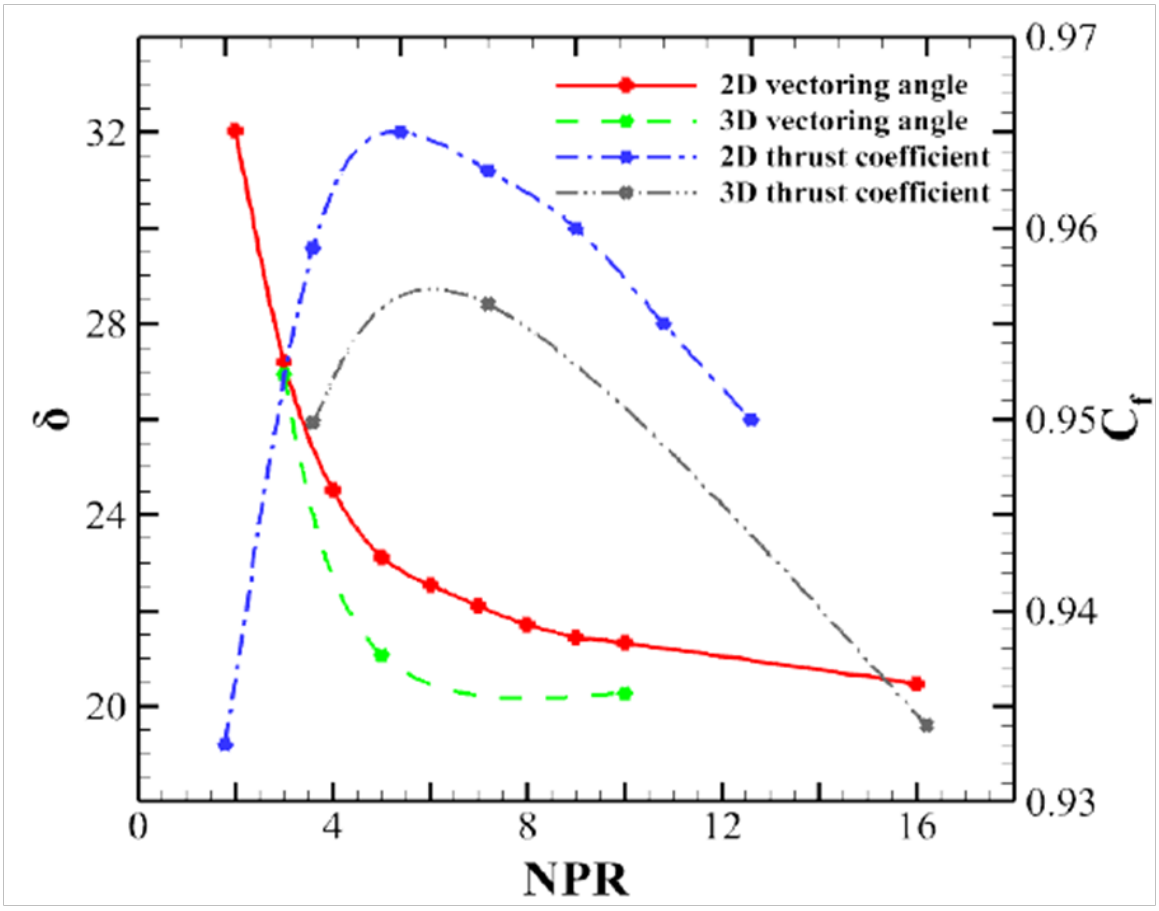

Figure 2.5: Effects NPR on δ and C_t on 2D and 3D BDTN configuration[15]

The table below summarize recent numerical investigation on BDTN configurations. It highlights various studies employing CFD, to analyze BDTN performance under different conditions, and examining the impacts of geometric parameters, flow conditions, and design variations on thrust vectoring characteristics.

Year	Title	Model	Varying Parameters	Computational Setup and Details	Conclusions	Ref
2014	*Experimental and Numerical Investigations of a Bypass Dual Throat Nozzle*	2–3D nozzle	NPR = 1–16	Fluent/realizable k-ε Model, 44,778 grid cells Pa = 101,325 Pa Ta = 300 K	NPR had a negative impact on TV angle. Thrust coefficient was found to decrease with increasing NPR. Best performance was recorded at NPR = 4.	[15]
2015	*Dynamic Experimental Investigations of a Bypass Dual Throat Nozzle*	3D nozzle	NPR = 3–10	Cold blowdown wind tunnel facility	At NPR = 3, 5, and 10, BDTN was able to achieve 50 deg/s, 40 deg/s, and 34 deg/s dynamic vector rate.	[16]
2019	*Computational study of axisymmetric divergent bypass dual throat nozzle*	2–3D nozzle	Expansion ratio = 1.1025–1.5625 Radius ratio = 1.05–1.25	Fluent/Spalart Allmaras Model 2.3×10^6 nodes Ppri = 455,300 Pa Psec = 607,950 Pa Pa = 101,325 Pa Ta = 300 K	The effect of radius of throat on TV performance was relatively small. Increasing the bypass width enhanced the thrust and discharge coefficients.	[26]
2020	*Design and Preliminary Analysis of the Variable Axisymmetric Divergent Bypass Dual Throat Nozzle*	3D nozzle	NPR = 4.47 i. After burning state ii. Non-afterburning state	Fluent/Spalart Allmaras Model 2.3×10^6 nodes Ppri = 453,138 Pa Psec = 453,138 Pa Pa = 101,325 Pa Ta = 2000 K Tin = 904 K	Non-afterburner state reported increased TV angles than afterburning states for both improve geometry scheme. Discharge and thrust coefficients were approximately equal for both nozzle states.	[27]
2020	*Experimental evaluation and numerical simulation of performance of the bypass dual throat nozzle*	3D nozzle	NPR = 2–16 Bypass position = 0.017	Fluent/RNG k-ε Model 855,000 grid cells Pa = 101,325 Pa Ta = 300 K	Increasing bypass position leads to increased TV efficiency. The thrust coefficient was reported in range of 0.85–0.93 with increasing NPR from 2 to 4.	[23]
2023	*Numerical Investigation on the Thrust Vectoring Performance of Bypass Dual Throat Nozzle*	3D nozzle	NPR = 2–10 Bypass angle = 35°–90° Convergence angle = 22°–37° Bypass width = 2.6–5 mm	Fluent/RNG k-ε Model Pa = 101,325 Pa Ta = 300 K	Increasing the bypass angle has a positive impact on vectoring angle and efficiency. Convergence angle has no significant impact on vectoring performance.	[30]

Table 2.3: Research gap of various BDTN design operation

By manipulating the flow rates and pressures of the primary and bypass streams, and by utilizing aerodynamic surfaces or fluid control within the nozzle, the direction of the exhaust jet can be altered to provide vertical lift components during take-off and landing. The cavity or mixing chamber located between the two throats plays a crucial role in the performance of BDTN, including the following:

- **Flow Mixing:** The efficiency of interaction and mixing of the high energy primary flow and the low energy bypass flow can influence the overall thrust and noise characteristics. Poor mixing can lead to thrust losses due to incomplete momentum transfer.

- **Pressure Distribution**: The development of complex pressure fields within the cavity due to the interaction of the streams and geometric constraints can influence the flow deflection mechanisms and overall TV capability.
- **Vortical Structures:** The shear layer between the streams can generate vortices within the cavity. With controlled generation and manipulation, these vortices can enhance mixing and improve the effectiveness of flow deflection surfaces. However, uncontrolled vortex shedding can lead to aerodynamic losses and noises.
- **Shock Wave Phenomena (at supersonic speeds):** In the case of supersonic exhaust condition, shock waves are formed within the cavity which lead to significant energy losses and affect the predictability of the flow deflection.
- **Boundary Layer Development:** With the development and behavior of the boundary layers along the walls of the cavity, the separation of flow and losses is influenced, particularly at high deflection angles.

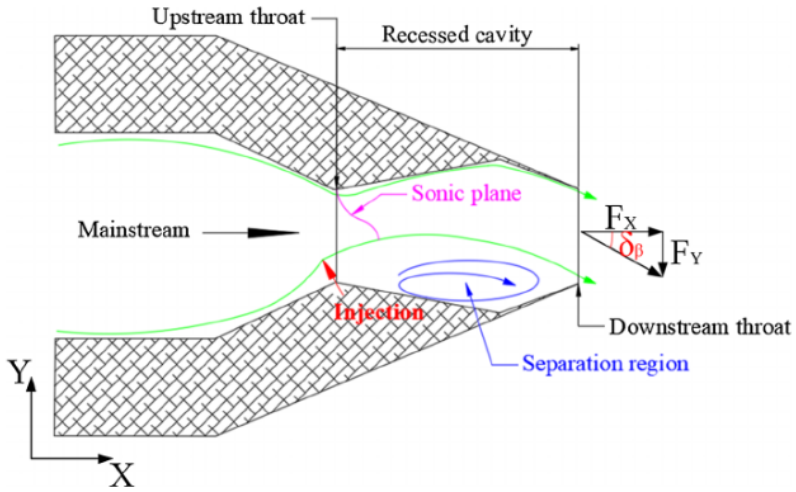

Figure 2.6: Schematic diagram of the principle of operation of Dual throat nozzle[12]

The above-mentioned phenomena can be observed in the experimental study conducted by Huang et al. (2022)[21]. The CFD investigation of the supersonic CD nozzle employs secondary air injection (SAI) into the divergent section of the nozzle[31]. The impact of various secondary injection parameters, such as injection angles and secondary air mass flow, on the thrust vectoring angle and the thrust efficiency of the nozzle at a nozzle pressure ratio (NPR) of 3. Using the $k-\epsilon$ RANS model to solve the Navier-Stokes equations for the compressible flow for the supersonic regime.
The numerical study showed a thrust vectoring angle of $\delta = 4.1°$ and a thrust efficiency of around $\eta_{thrust} = 98.5\%$ at an injection angle of $\alpha = 30°$. The effects of NPR , secondary pressure ratio (SPR), injection location β and injection angle α with respect to C_t and δ, is represented graphically in the Figure 2.5. On increasing NPR

the δ decreases marginally, but the C_t reaches its peak before falling to an almost constant value[32]. While, for increasing SPR the behavior of δ is opposite and C_t is observed to decrease linearly. The vectoring angle α increases parabolically with it maximum value reaching closer to primary throat, having the highest thrust coefficient $C_t > 0.95$ while vectoring angle δ decreases .

This deep understanding can guide the research directions of the current project and support the achievement of its objectives. The design of bypass dual throat nozzles, thrust vectoring with the supersonic nozzle, and optimization of the nozzle design with respect to STOL performance should be further investigated. To overcome the gap, the team has considered injecting 3 to 9.57% secondary mass flow through a curved conduit to ensure proper mixing of the exhaust flow, with controlled pressure injection at low flow speeds. This allows the controlled vortical structure formation with shock and boundary layer development to add to δ , thrust vectoring angle, in the selected BDTN configuration.

The team has also conducted an investigation of the design performance of the BDTN configuration for different phases of flight, such as take-off, cruise, and landing. Thus, we investigate the variation of the mass flow rate under the assumption of an ideal mixing condition in the exhaust and the variation of the secondary injection angle α maintaining a selective mass flow rate. The study has been carried out to understand the flow behavior in the BDTN performance like the effects on thrust coefficient C_t, thrust losses and thrust deflection angles both in vertical and horizontal (δ_v and δ_h) at an optimum design configuration.

Chapter 3

Numerical Methodology

The fighter aircraft have three general phases of flight namely, Take-off, Cruise and landing, depending on different mission profile and requirements, some additional trails can be added. The Osprey mission profile is represented in Figure 3.1. With capabilities like super maneuverability, STOL and high payload capacity of such aircraft, it became crucial, especially during combat scenarios due to faster response rate and high performance graph.

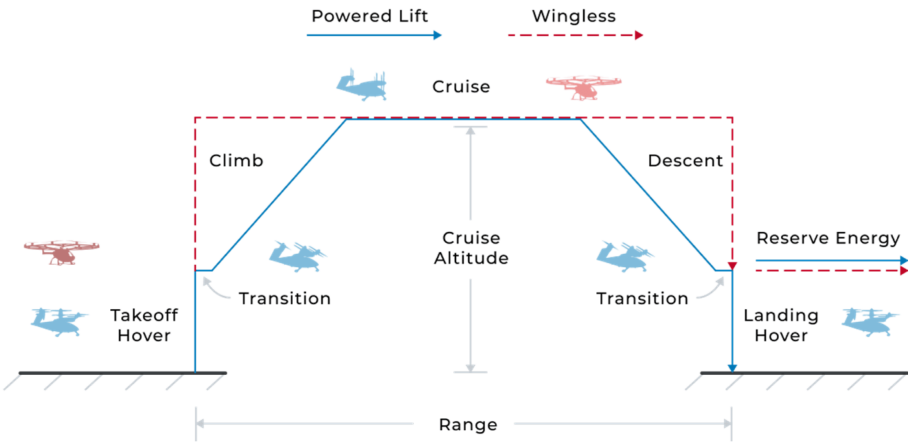

Figure 3.1: V-22 Osprey Simple Mission Profile for VTOL[33]

The transition from powered lift and wingless flight has been a significant study in the research of Huang et al.[20,21]. With proper CFD ANSYS models, the flow behavior analyzed showed the reduced time rate for the transition of the turboprop from powered to wingless flight in V-22. A sophisticated numerical tool, CFD-ANSYS FLUENT is employed to analyze and predict flow-related physical phenomena. This involves a systematic approach to numerically solving the governing equations of fluid flow and behavior. The project has been carried out for the take-off and cruise phase segment of the fighter jet to analyze the engine exhaust performance upon incorporation of the mentioned FTVC technique to achieve STOL operation.

3.1 Pre-Processing

3.1.1 Geometry Model

The computational model for BDTN was designed with reference to the model described in the study conducted by Huang et al.[20,21], utilizes the percentage of primary flow bypass stream in the nozzle exhaust, is termed BDTN, thus changing the flow properties of the injected primary flow. This internal injection of the primary stream without external components results in a thrust vector coefficient with some deflection angle δ. This δ can then be controlled with the use of valve actuators in the conduit. The geometry of the BDTN constructed on Design Modular - ANSYS, considered for the numerical investigation, is shown in detail in Figure 3.2.

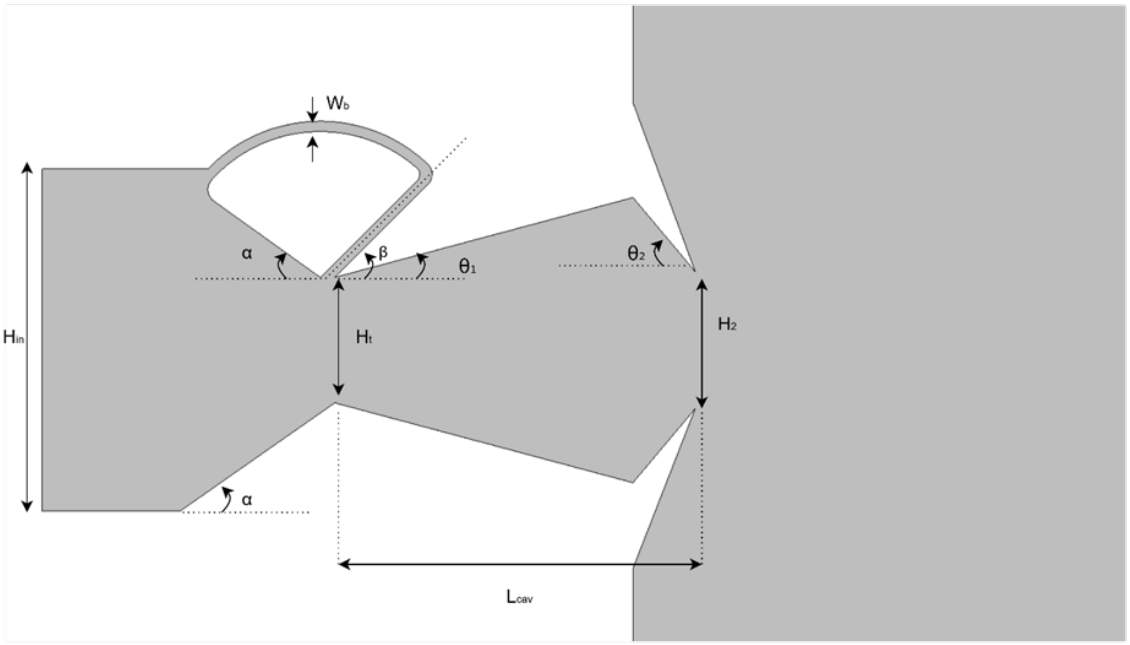

Figure 3.2: BDTN Configuration

The quantification of the non-dimensional geometry parameters is shown in Table 3.1 below. These quantities are with reference to the investigation study for a V-22 turboprop engine, with minimal variations, which are considered according to the fighter jet engine for STOL capabilities.

H_{in}/H_t	H_2/H_t	L_{cav}/H_t	W_b/H_{in}	H_f/H_{in}	L_f/L_{cav}
2.72	1.09	2.88	6.16%	4.67	3.88

Table 3.1: Non- dimensional geometry parameters of optimized BDTN exhaust system for STOL.

The working state of the engine is reduced by diminishing the external redundant components used in other FTVC techniques. The proposed exhaust system is considered to be installed as a conventional jet engine, which has not been considered in the study by Huang et al.[20]. It is important to understand that all angles in this study are positive when calculated from the horizontal axis of the first quadrant; the negative sign shows that the calculation of the same is carried out from the negative axis or the horizontal axis of the second quadrant. The BDTN exhaust system, consisting of a curved conduit with injection angle $\beta_1 = 45°$, having first convergence angle $\alpha_1 = 30°$, with progression of divergence section at angle $\theta_1 = 15°$ and second convergence at $\theta_2 = -50°$. With an expansion ratio (E_r) of 1.2 and bypass inlet width (W_b) of 6.16% of primary inlet diameter or height (H_{in}). The ratio of primary inlet diameter, secondary throat diameter (H_2) and cavity length (L_{cav}) to throat inlet diameter is mentioned in Table 3.1. This 2 D computational model consists of the presence of a far field to analyze the behavior of the exhaust plume in an ambient environment, which is depicted in Figure 3.3.

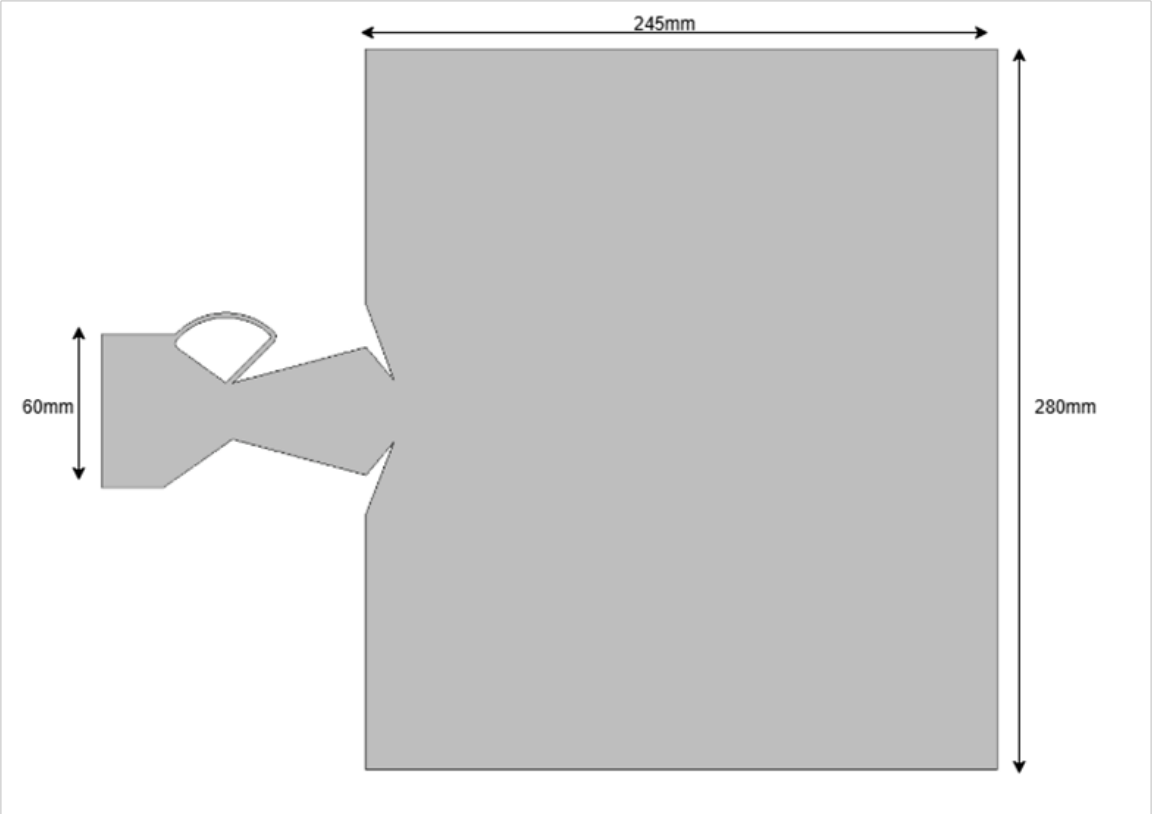

Figure 3.3: Far field environment configuration

Measurements are considered in millimeters for the proposed geometry for computational ease as the ANSYS- Fluent software in default settings, understand this unit of measurement of geometry. The far field height ratio, (H_f/H_{in}) along with the far field length ratio (L_f/L_{cav}), is mentioned above in Table 3.1.

This investigation is conducted in two sections to select an optimized geometry with high STOL performance. Section A: investigates the geometry with varying W_b/H_{in}: 3%, 6.16% and 9.51% each with NPR of 1.5, 3 and 4, keeping a constant injection angle, $\alpha_{inj} = 45°$. The STOL performance parameters were investigated to achieve the optimal operating conditions for the BDTN exhaust system, the geometries of which were constructed using Design Modular of ANSYS as shown in the Figure 3.4 below.

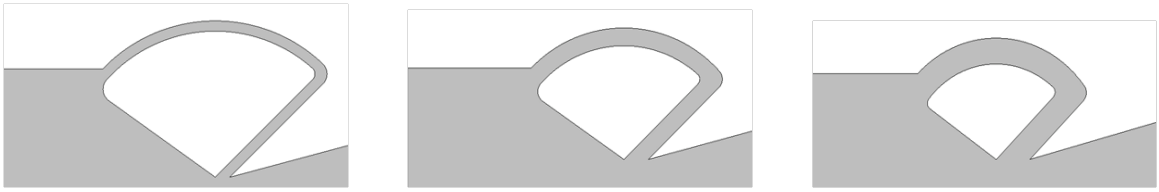

(a) $W_b = 1.7mm$ **(b)** $W_b = 3.7mm$ **(c)** $W_b = 5.7mm$

Figure 3.4: Bypass conduit configuration with varying W_b

Upon analysis of Section A for the optimal operating conditions, the variation of injection angle (α_{inj}) from 30° to 75°, for constant NPR and conduit width (W_b) of 4 and 6.16% respectively. The geometry near the conduit is shown in Figure 3.5 below.

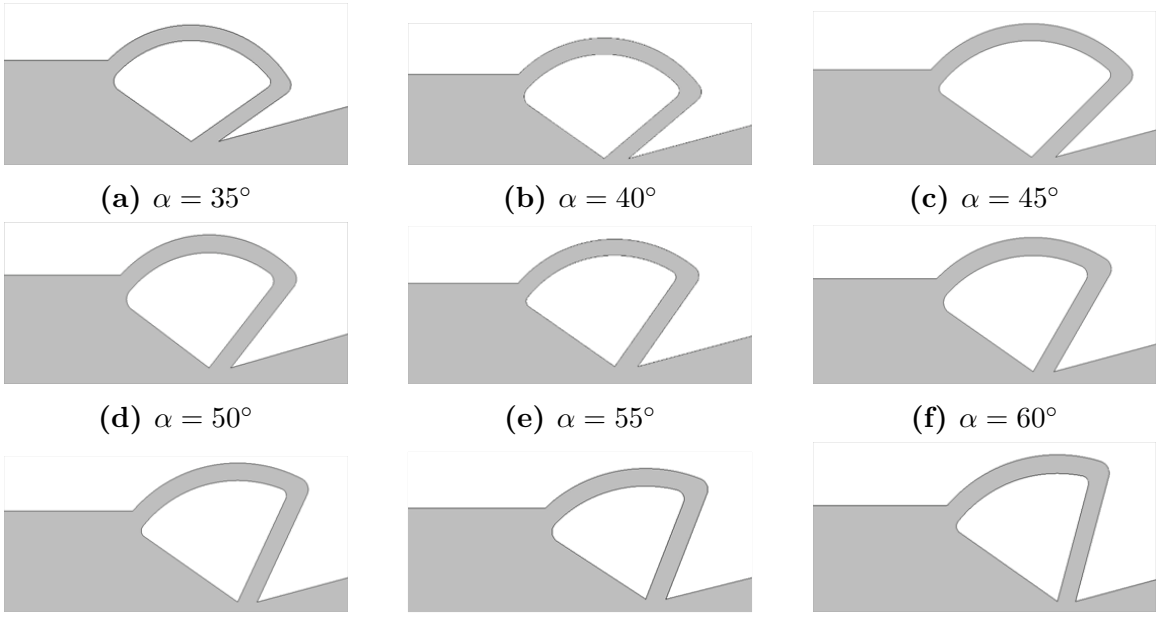

(a) $\alpha = 35°$ **(b)** $\alpha = 40°$ **(c)** $\alpha = 45°$

(d) $\alpha = 50°$ **(e)** $\alpha = 55°$ **(f)** $\alpha = 60°$

(g) $\alpha = 65°$ **(h)** $\alpha = 70°$ **(i)** $\alpha = 75°$

Figure 3.5: Bypass conduit configuration with varying α

These 2 D BDTN configurations were then taken further in the pre-processing stage of the computational modeling, which is grid or mesh formation.

3.1.2 Grid Generation

Meshing transforms a continuous physical problem into a discreet one by making it solvable using the finite volume numerical method (FVNM) used by CFD-ANSYS. The proposed geometry contains a structured 2D mesh grid as shown in the Figure 3.6 below. This makes the mesh more efficient for higher accuracy, allows faster convergence, and requires a lower computational cost.

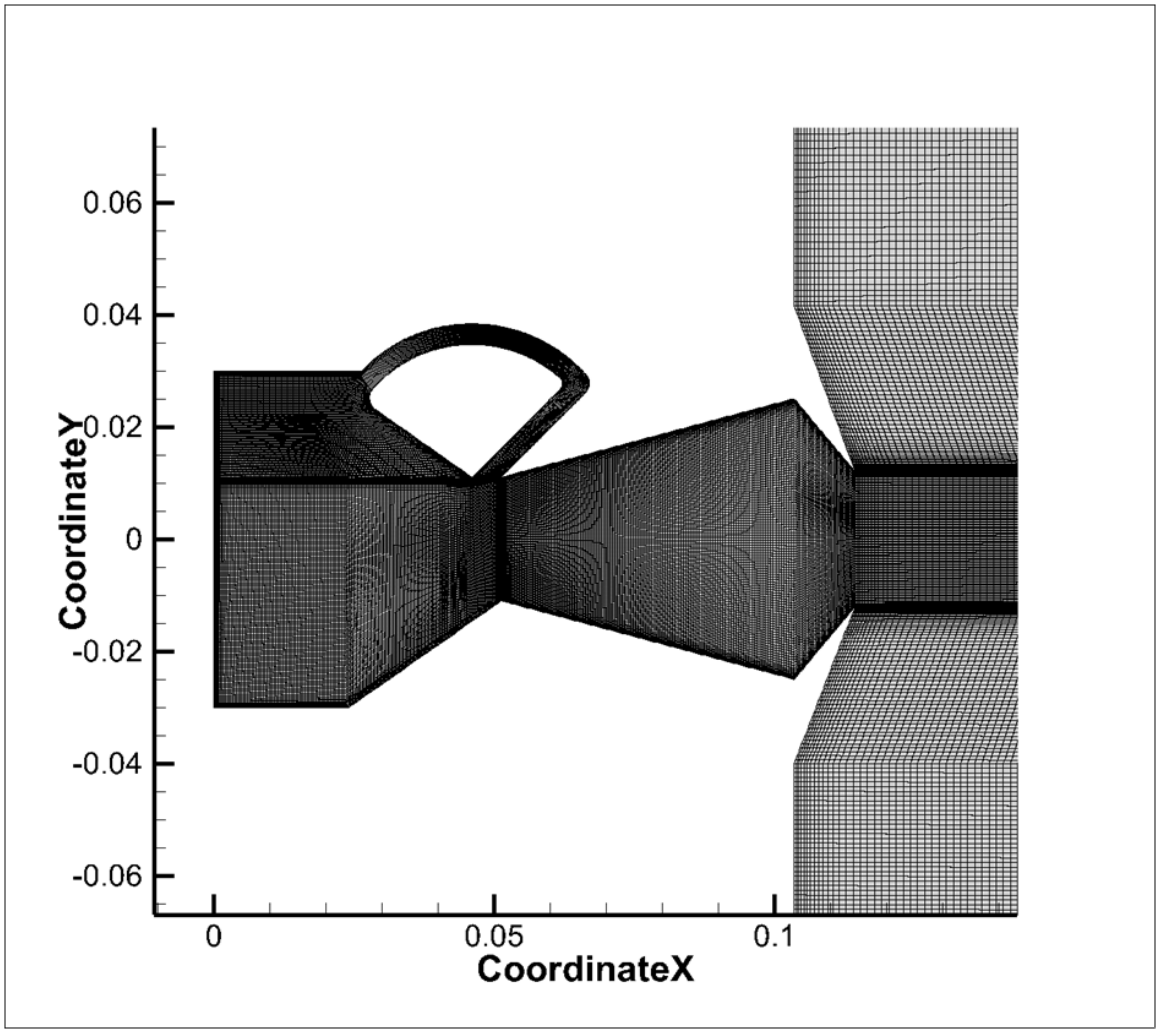

Figure 3.6: Grid generation for the BDTN configuration

The geometry domain is divided into smaller elements called cells with defined nodes, faces, and edges. To obtain accurate results from the mesh, it is important to ensure that the four main mesh parameters are within the optimum range to produce the desired results with the minimum possible error during discretizations. Thus, these are well maintained under the standards, throughout the mesh, for optimum computational investigation. The structured mesh is shown below.

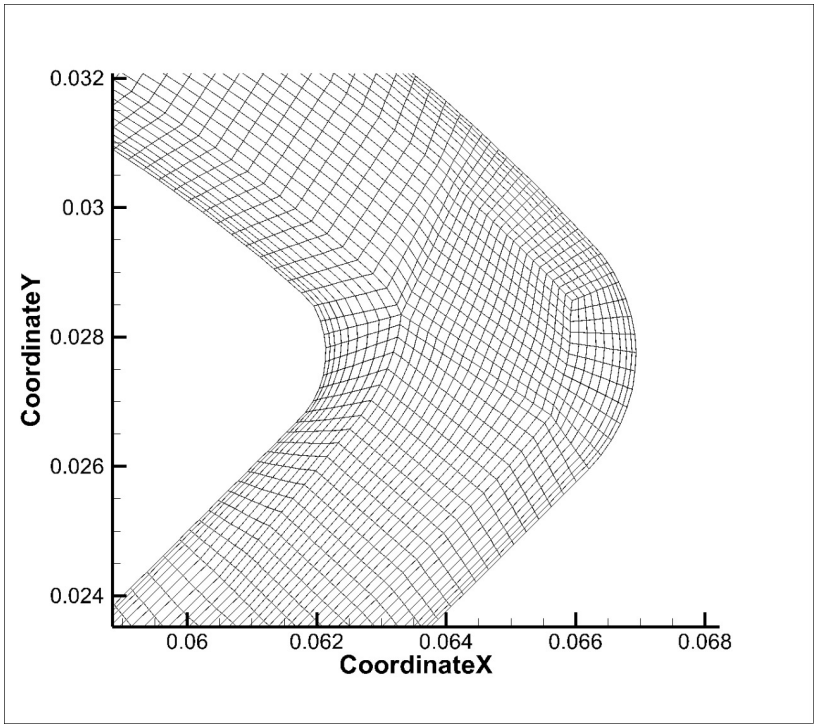

Figure 3.7: Bypass Conduit structured grid

The standards considered are mentioned in Table 3.2. These standards allow better control over mesh quality parameters such as cell shape, aspect ratio, and orthogonality, which are crucial for solution accuracy and stability. The creation of highly stretched, well aligned structured layers near the solid walls makes them well-suited for resolving viscous sub layers in turbulent flows using the wall functions or low Reynold's number models, which is discussed in the next section.

Parameters	**Range**
No. of elements	1.5 Lakhs
Y+ wall Distance	Less than 10
Cell Volume change	Less than 2
Orthogonal Quality	Greater than 0.35
Max Aspect Ratio	Less than 50

Table 3.2: Considered mesh parameter standards

3.1.3 y^+ Wall Distance

It is a dimensionless wall distance that is used in CFD to describe the size of the first cell adjacent to a wall in turbulent flows. It is a crucial parameter for determining the accuracy with which the near-wall region, particularly the turbulent boundary layer, is resolved by the computational mesh.

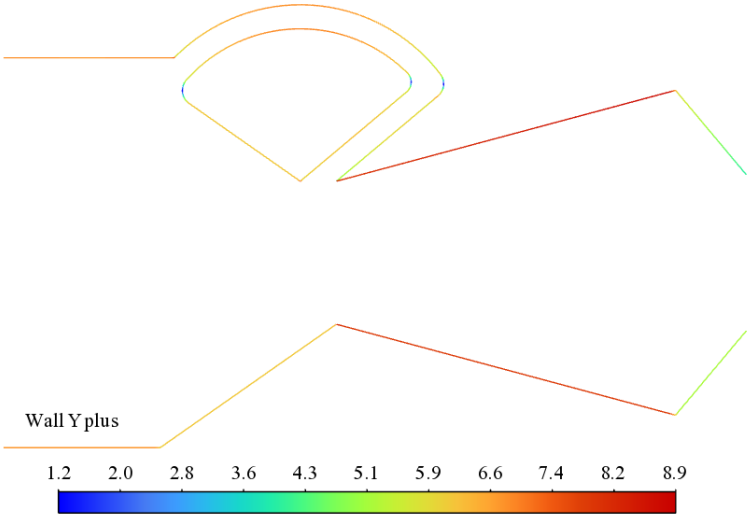

Figure 3.8: y^+ wall distance of BDTN configuration

When a viscous flow is simulated, a boundary layer is formed near the walls. Here, the moving fluid meets the no slip condition and the flow at the wall becomes zero. This results in a parabolic velocity inlet in the fully formed region. In order to obtain the exact velocity magnitude in the vicinity of the wall, the cell center distance of the first layer adjacent to the wall must be small enough to capture the details. The equation that follows for the calculation of this dimensionless wall distance is given below:

$$y^+ = \frac{Y_p U_\tau}{v} \text{ and } U^+ = \frac{U}{U_\tau}$$

Here,

- y_p: distance normal to the wall where y^+ is calculated
- U : velocity parallel to the wall as a function of y,
- U_τ: Shear velocity or friction velocity near the wall,
- v: Kinematic viscosity.

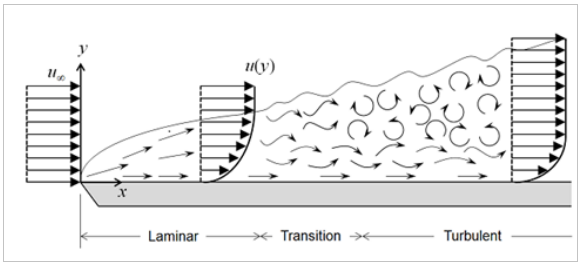

Figure 3.9: Wall Shear Layer distribution[34]

Figure 3.9 shows the variation of y^+ wall distance corresponding to the U^+ wall distance. The figure 3.10 shows the direct numerical solution (DNS) data, which accurately depicts the experimental data, including internal and external viscous flow, that follows the trend when plotted along U^+ and y^+ distance. As the viscous sub layer accurately predict y^+ less than 5 and in range of 20 to 200, also known as the log law region is modeled well. However, for y^+wall distance between 5 to 20, there is a buffer region and both the linear model and the logarithmic model is inaccurate corresponding to the actual DNS data.

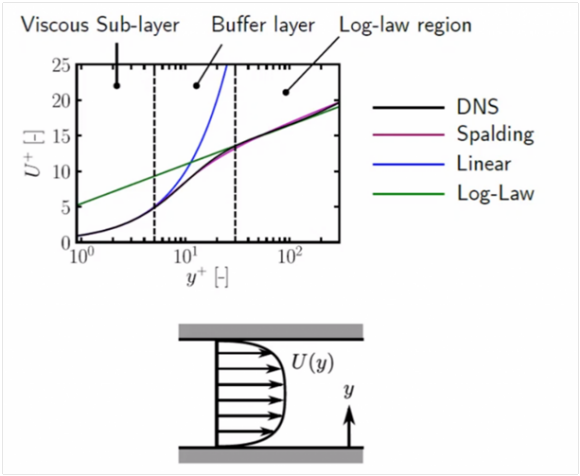

Figure 3.10: Effect of different numerical methods on U^+ wall distance[34]

Therefore, it is vital to keep the edge parameters in mesh such that the y^+ distance of the wall should lie within 10 or in range of 20 to 200 to obtain meaningful and reliable. Otherwise, it will lead to computational results which are non convergent in nature.

3.1.4 Orthogonal Quality

It is a metric parameter that quantifies the closeness of mesh cells resembling ideal orthogonal shapes. A perfect orthogonal mesh has cell faces that are perpendicular to each other. It is typically represented by a value ranging from 0 to 1, where 1 indicates perfect orthogonal cell and 0 represents non-orthogonal or degenerated cell.

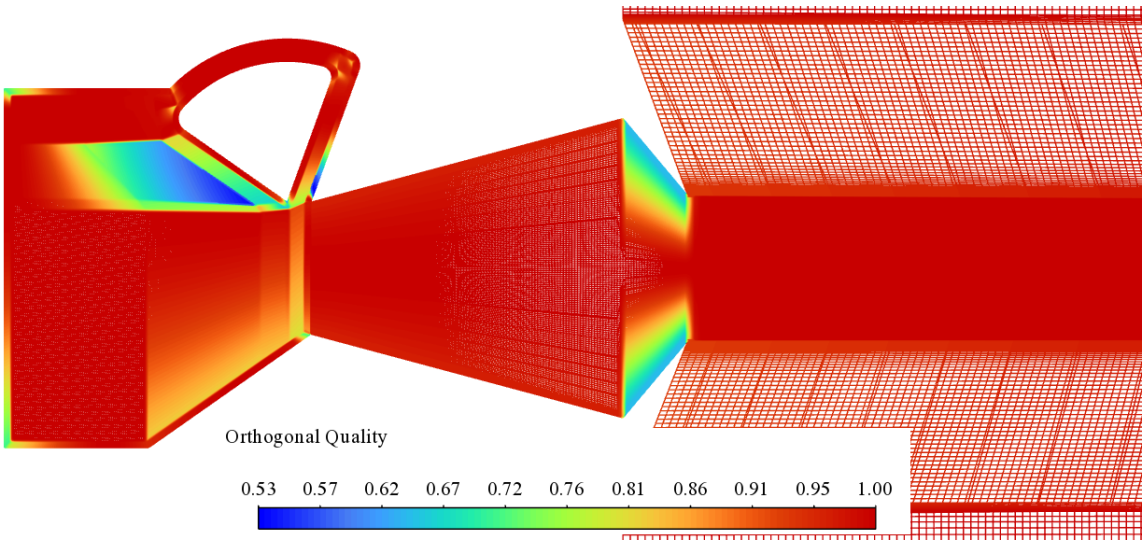

Figure 3.11: Orthogonal Quality of the mesh

Since the acceptable range for orthogonal quality generally aimed for values above 0.1 or 0.2. In the computation model the team has achieved a minimum cell orthogonal quality is maintained above 0.4. It is often calculated based on the angle between the vector connecting the centers of the two adjacent cells and the normal vector of the face they share as represented in the figure below. Deviations from a 90° angle reduce the orthogonal quality.

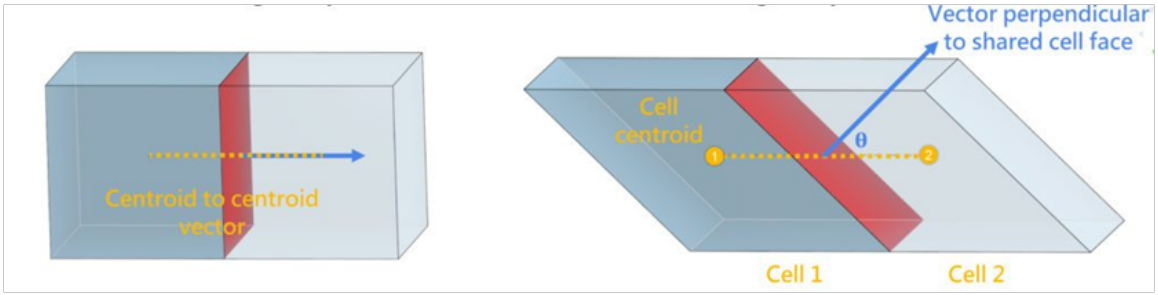

Figure 3.12: Concept of Orthogonality in Cell[35]

It is crucial metric for evaluating the suitability of the computational mesh, which helps ensure the accuracy, stability, and the convergence of the numerical solution for a good orthogonality.

3.1.5 Aspect Ratio

It is a measure of the distortion of a cell compared to an ideal or equilateral shape. It is defined as the ratio of the cell's longest characteristics length to its shortest characteristics length. An aspect ratio of 1 represents an ideal, equilateral or equiangular cell (example, a perfect square or cube). As it increases the cell becomes stretched or elongated. While some stretching can be acceptable and even beneficial in specific regions (like boundary layers aligned with the flow.

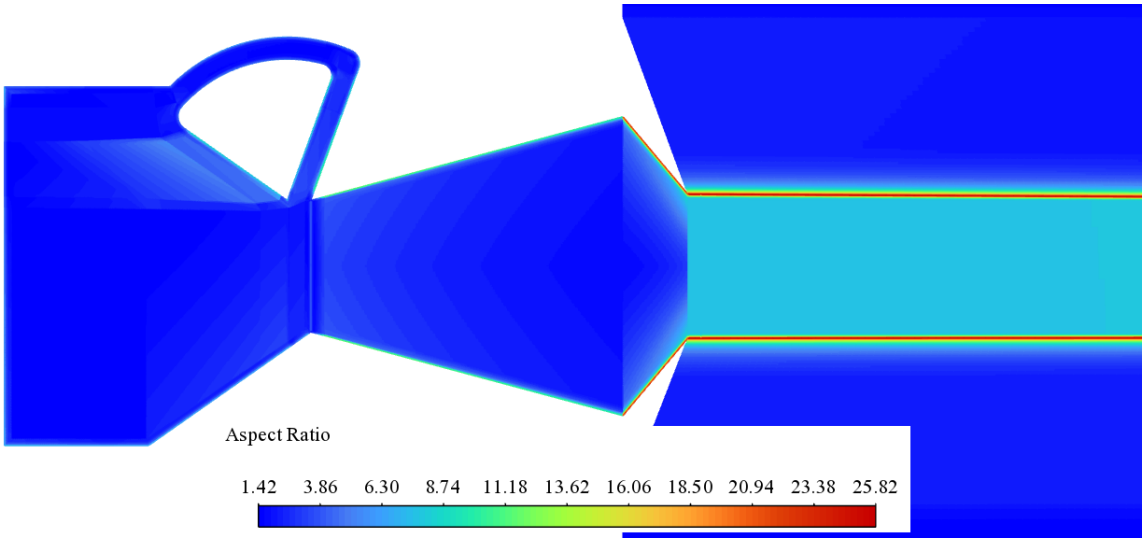

Figure 3.13: Aspect Ratio of mesh

Upon applying a wall distance of 0.05 mm with the H_{in} of 60 mm in the BDTN configuration resulted in a y^{+}wall distance under 10 while the aspect ratio reaches around 40. Had the aspect ratio touched unacceptable range in multiples of hundreds, the team would have then chosen a y^{+} wall distance between 20 to 200, to achieve a lower aspect ratio in the region formed by crossing of concentrated vertical cell height near nozzle exit and the horizontal cell height in far-field.

3.1.6 Cell Volume Change

It refers to alterations in the volume for computational cells during a simulation. This phenomenon can occur intentionally due to adaptive mesh refinement (AMR) or dynamic meshing, or unintentionally as a result of poor mesh quality or numerical instability.

Fluent solves the CFD using Cell-Volume Method. Therefore difference in volume across adjacent cells becomes critical and it often leads to faulty results if cell volume change across blocks are larger. Ideally cell volume change should be close to 1. The mesh has been maintained under a maximum cell volume change region within 0.75 to 2.1. This can be ensured while blocking by following three methods :

1. Decreasing no. of nodes in denser blocks or increasing no. of nodes in sparse region

2. Moving vertices while blocking so that denser blocks become longer and sparse blocks become shorter

3. Applying edge parameters in two blocks having a shared face, with a growth ratio within 1.00 to 2.00.

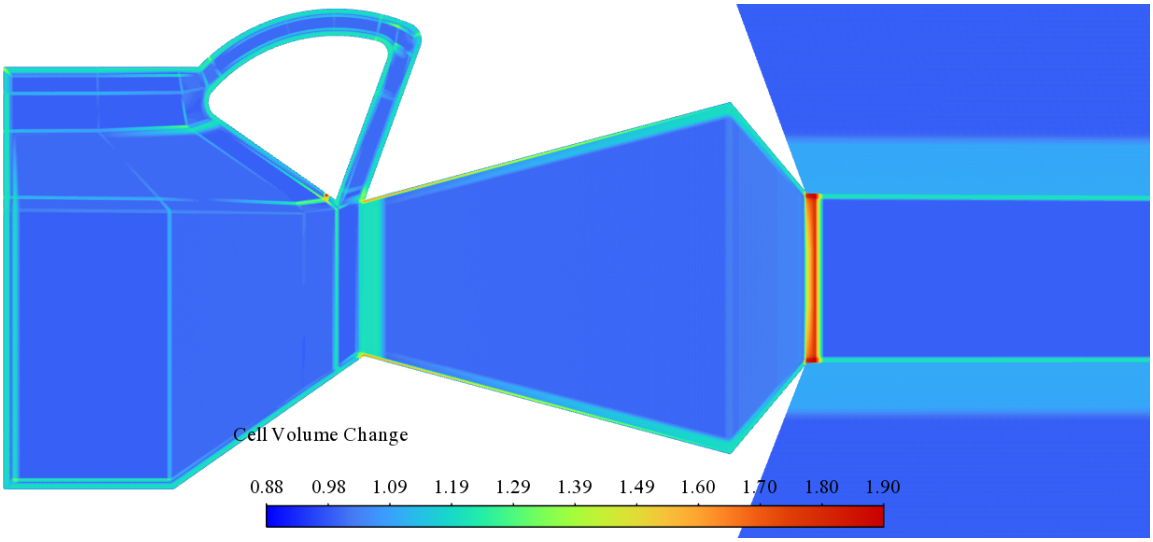

Figure 3.14: Grid cell volume change

3.1.7 Blocking

It is a technique primarily used in the generation of structured meshes, especially for complex geometries. It involves diving the computational domain into a set of similar, interconnected blocks. Each of which is then meshed independently with a structured grid consisting of quadrilateral cells in the 2 D BDTN geometry design.

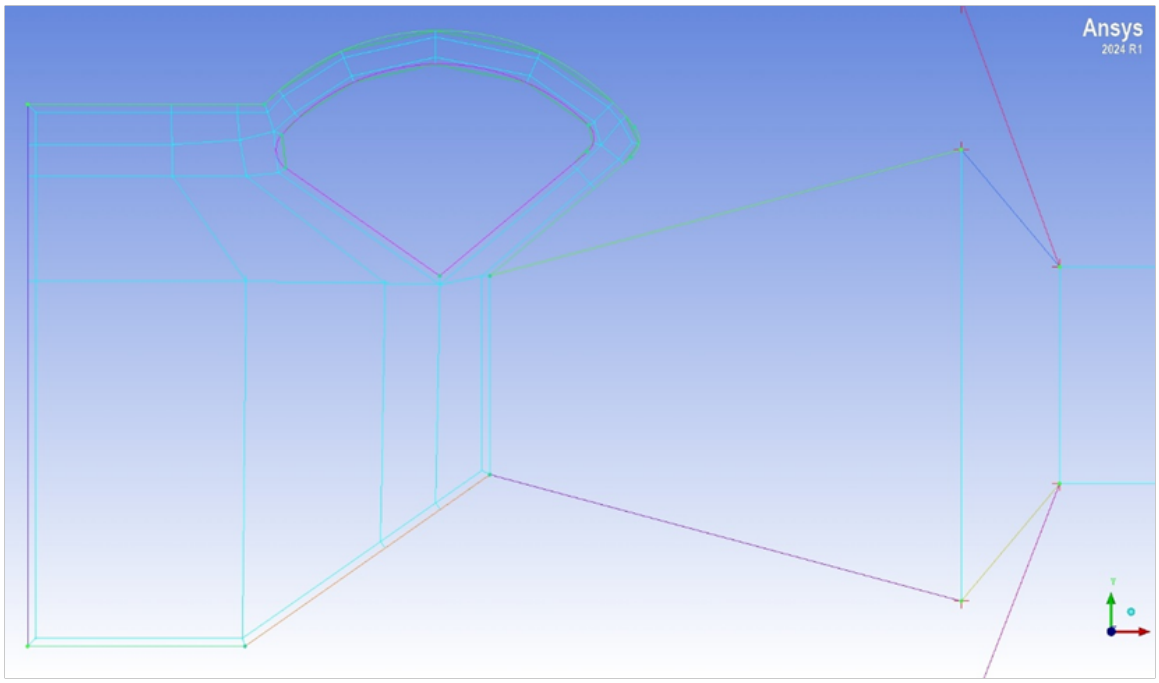

Figure 3.15: Blocking in BDTN configuration

The final blocking pattern which has been used to balance the various quality parameters, is shown above. Blocking ensures that the complex geometries are handled by breaking them into topologically simpler blocks and the quality of the mesh is

improved. It facilitates local mesh refinement by controlling number of cells within specific blocks, especially near walls, in shear layers or around complex geometry features, where higher resolution is needed.

The common blocking strategies that the team considered to obtain the desired mesh quality includes the following :

- *O-grid*: it is used for internal flows or flows around circular or bluff bodies, by creating a central block surrounded by concentric layers of cells
- *C-grid:* it is often used for external aerodynamic flows, wrapping around lifting surfaces with a wake region extending downstream.
- *H-grid:* it is a straight-forward block structure often used for rectangular or ducted flows.
- *Y-grid:* it is used for handling sharp corners or leading/trailing edges.

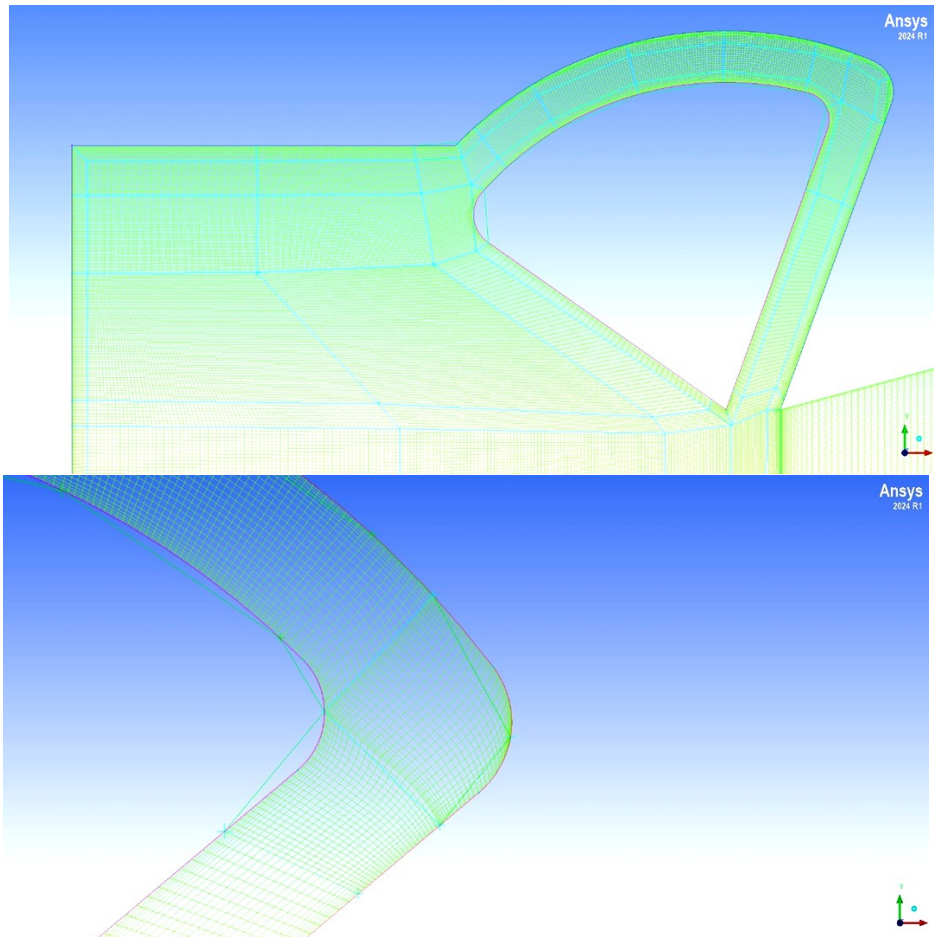

Figure 3.16: Blocking using O-grid strategy

The investigation is carried out by the O-grid blocking technique to ensure that

the high mesh quality is not compromised and the computation yields quality results. The BDTN mesh components can be observed in detail in the figure below.

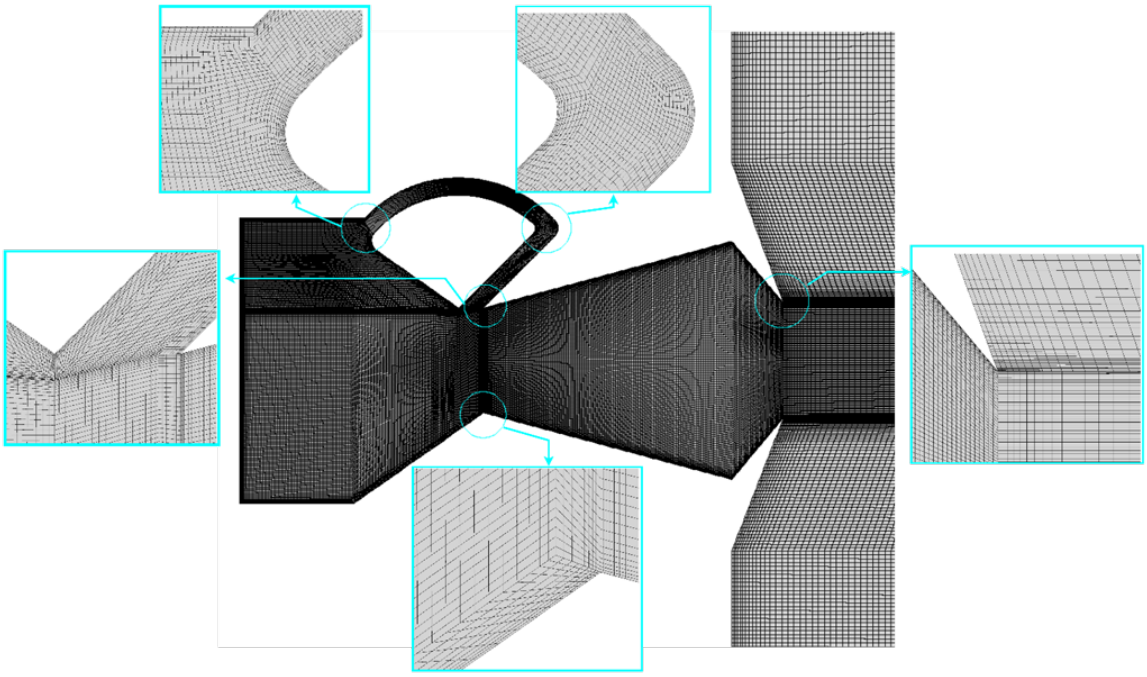

Figure 3.17: Structured mesh through O-grid

3.2 Solver Set-Up

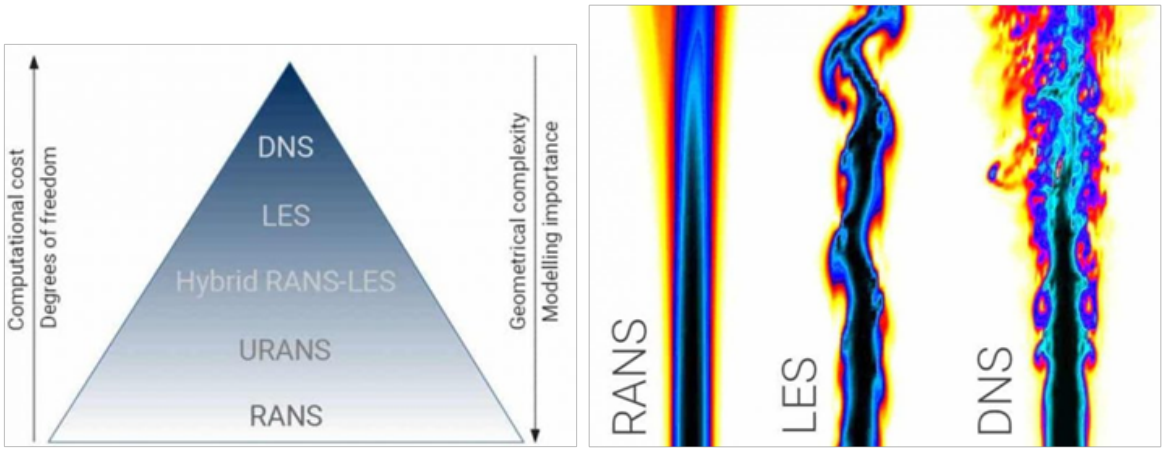

(a) **(b)**

Figure 3.18: (a). Pyramid of Computational Models[36] (b). Computational comparison of RANS, LES and DNS[36]

It is a crucial stage after pre-processing where the numerical engine is configured to solve various fluid flow statements. The Fluent solver is set up as density-based. Since the focus of the study is to obtain an average flow deflection angle δ, at the exhaust exit, a turbulence model is selected which requires less computational cost

and provides decent accuracy. Therefore, Reynold's averaged Navier Stokes (RANS) model is an appropriate selection according to the hierarchy of computational models.

The Realizable $k-\epsilon$ Model with standard wall function to achieve the desirable flow behavior. Roe's flux difference splitting scheme (RFDSS) and the second order upwind are adopted to discretize the inviscid and viscous flux terms on the control volume surfaces in the realizable $k-\epsilon$ equation. The energy equation has been involved, and air has been taken as the ideal gas to model the internal gas flow inside the nozzle with the assumption of complete mixing in the exhaust. The Sutherland law has been used to calculate the dynamic viscosity. The detailed setup of the solver, along with the governing equations, can be accessed in Appendix A.

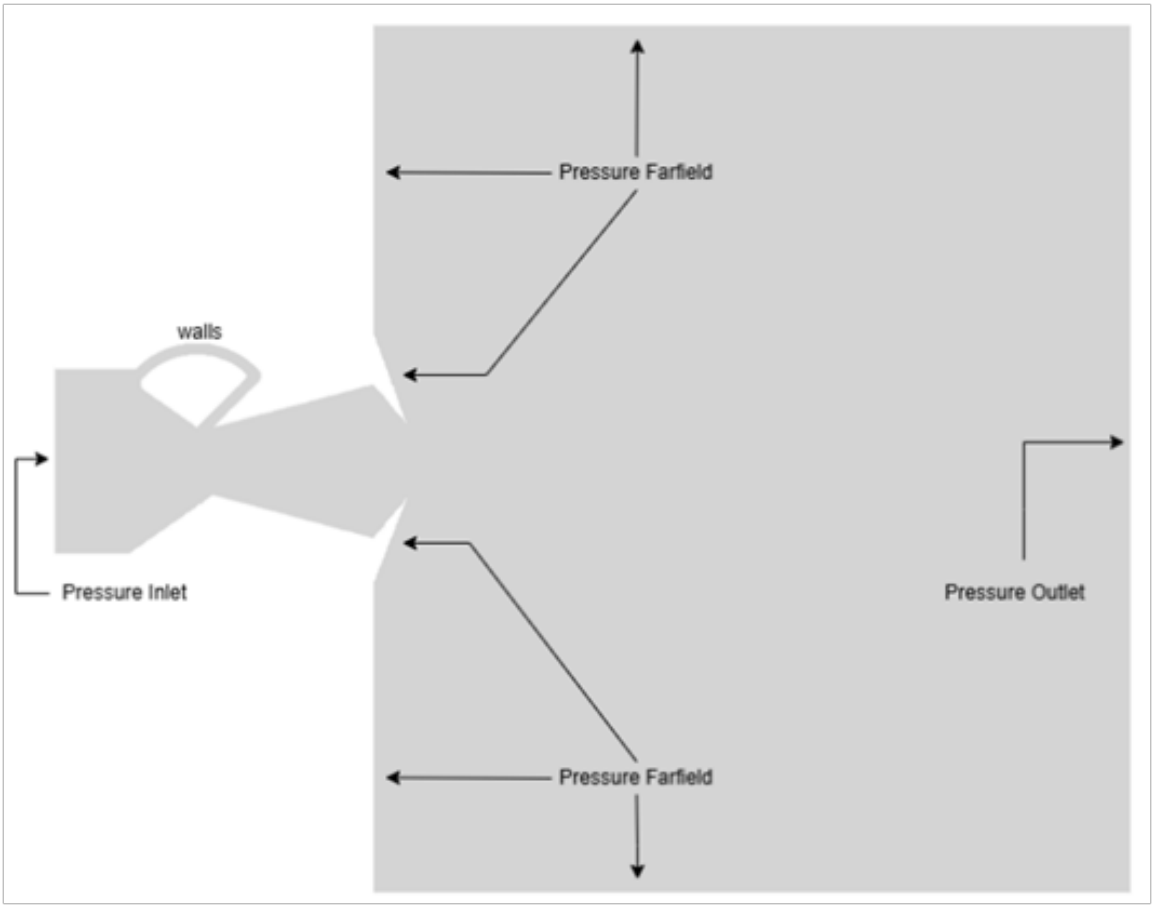

Figure 3.19: Computational Domain of BDTN configuration

After setting the solver, the calculations are initiated based on certain boundary conditions that monitor the domain environment for which the computation is carried out. The solver then iteratively solves the discretized equations, mentioned in Appendix A, until the convergence criterion is met for steady state or specific simulation time is reached for transient condition. The following Boundary Condition has been adopted to study the flow field.

Inlet Conditions Type	Pressure
Total Pressure (P_o)	$405300Pa$ (NPR = 4)
Inlet velocity(V_{in})	64 m/s
Turbulent intensity	3%
Static Temperature	$300K$
Outlet Conditions	
Total ambient pressure (P_{amb})	$101325Pa$
Turbulent intensity	5%
Turbulent viscosity ratio	10%
Static Temperature	$300K$
Far Field Conditions Type	Pressure
Gage Pressure	$101325Pa$
Velocity	set to 0.01 Mach number (Ma)

Table 3.3: Computational Domain Boundary Condition.

The P_o is considered for Section A of the investigation, where the inputs included are: $405300Pa$ (NPR 4), $580000Pa$ (NPR 5), 151987.5 Pa (NPR 1.5). The supersonic/initial gauge Pressure has been chosen for each NPR where the inlet velocity is same, i.e. $64m/s$. Thus, ensuring the same mass flow rate in Section B of the study. The turbulence conditions for the intensity and hydraulic diameter have been chosen to set the turbulence conditions at the inlet. Since air flow is mostly streamlined, the expected turbulence is less, therefore, turbulent intensity has been assigned a value of 3%.

The turbulent condition at the outlet is set on the basis of the backflow turbulent intensity and viscosity ratio, mentioned in the above table. The operating pressure for the far field is set to 0, since all the pressure terms have been written in the form

of total pressure, and the back pressure is 101325 Pa itself, as mentioned in the table.

3.2.1 Courant Number

It indicates how much information from the flow variable travels through a unit cell in a unit time. If courant number is one, and time step size is adjusted such that information travels at the speed of 1 cell in unit time step size. If Courant number is 0.5, information passes at half the length of an unit cell in 1 time step size. If the inlet velocity is higher, the time step size decreases to adjust the inlet speed.

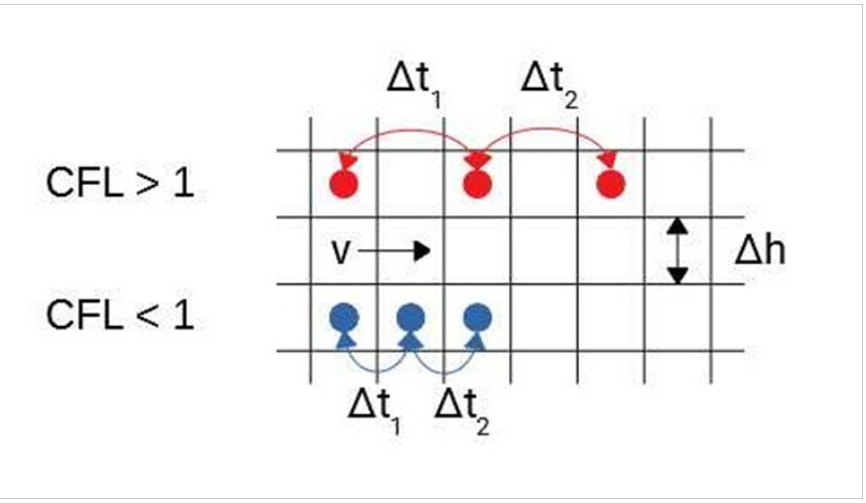

Figure 3.20: Concept of Courant Number[22]

For the study, the courant number is taken as 0.5 in all cases. Since our simulation deals with internal flow and it becomes highly turbulent aft of throat and there is eddies formed, we required our time step size to be small enough to capture all the details. All the numerical setups have been initialized from inlet and 60,000 iterations have been run in order to converge all the results.

3.2.2 Convergence Criteria

It is a set of conditions that a numerical solution must satisfy to be considered adequately to converge to the true solution of the discretized governing equation. Since CFD is an iterative process, these criteria determine when the iterations should stop. Achieving proper convergence is crucial to obtain physically meaningful and reliable computational results. The convergence criteria of the study is based on the wall pressure , as shown in the figure below.

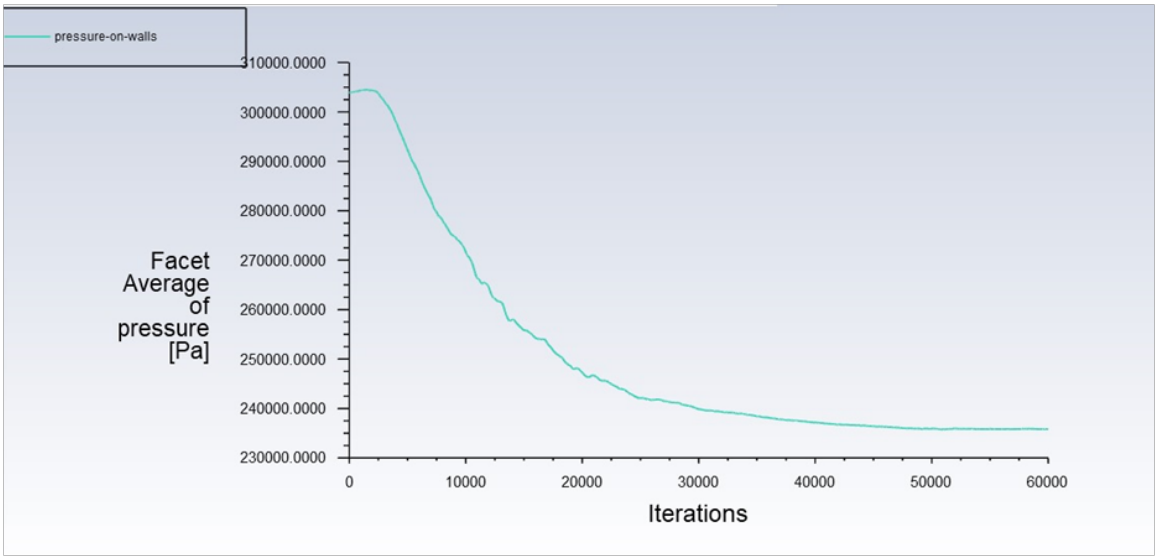

Figure 3.21: Convergence criteria: Pressure on walls

Pressure on walls has been plotted against the number of iterations to judge whether the results are converging or not. In the turbulent model, Reynolds number is very high, and accuracy of flow variables such as continuity equation, x-velocity, y-velocity are in the accuracy of 2 decimal places, whereas k and ϵ are accurate up to 4 decimal places according to residual data. Therefore, residuals alone would not be sufficient to judge whether the result has converged or not. A new criterion has been added to the report of the facet average pressure on walls, which records the data at every 1 iteration. A constant value suggests that further calculations will lead to a consistent value in the exhaust, thus converging the numerical solution of the flow.

Chapter 4

Result Discussion

Following, the rigorous computational methodology delineated in the previous chapter, this chapter is dedicated to the exposition of the resultant findings derived from the numerical simulations undertaken to comprehensively investigate the performance of the optimized BDTN configuration. The ensuing sections will meticulously present the quantitatively analyzed data pertaining to the two sections of the study conducted, after validation of the flow parameters like the pressure and shear wall stress from the computational methods. This is discussed in detail in the ensuing section.

4.1 Validation

To establish the credibility and accuracy of the CFD methodology employed in this study, a rigorous validation process was undertaken. This section presents a comparative analysis between the numerical results obtained from the developed CFD model and established benchmark data available in the open literature for DTN case of different flight modes[20,21]. Its important to observe that the validation geometry for this project is different from that of the benchmarks' and hence only the flow behavior trend is represented and compared for further study of the BDTN configuration.

The primary objective of this validation exercise is to quantify the fidelity of the chosen numerical schemes, turbulence model, and boundary condition implementation in accurately predicting the key flow parameters like the pressure ratio, pressure coefficient (C_p) and shear wall stress(τ_{wall}). These graphs were generated upon extracting the data files from ANSYS and from image processing technique from the benchmark study[20,21], to obtain data, which was then plotted in ORIGIN Pro for the purpose of validation. From the graphs it becomes evident that the trend is followed by the proposed optimized BDTN configuration.

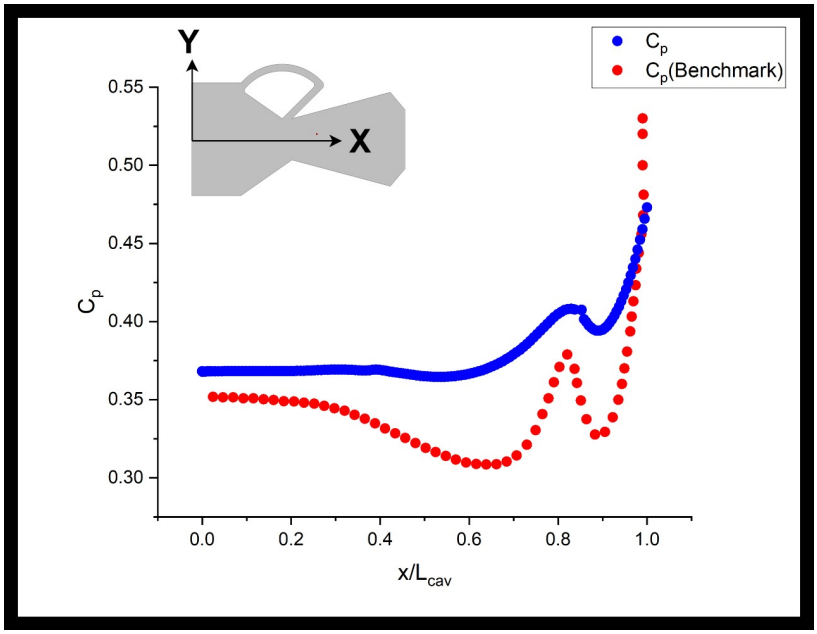

(a) Comparison of pressure coefficient of the lower wall of BDTN configuration

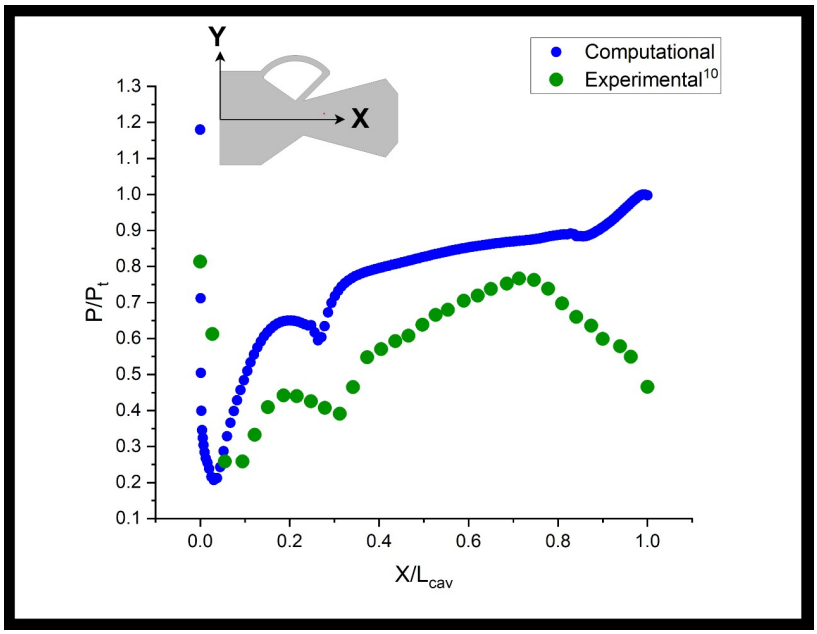

(b) Comparison of pressure ratio at the lower wall of the BDTN configuration

Figure 4.1: Experimental-computational validation of BDTN

The flow behavior is graphically represented to understand and compare the flow parameters like pressure and shear wall stress. The exhaust velocity achieved from the computational methods in the mentioned study was in the range of 120 to 240 m/s, while for the current project investigation the exhaust flow velocity lies in the range of 110 to 400 m/s for the operating condition of NPR 4.

For a detailed computational study, the optimum flow conditions were set as a the first case segment, which is discussed in detail in the next section. Upon successful comparison and noted trends which are observed to be similar for both the benchmark

and the proposed design configuration, the study of thrust performance in the exhaust system was conducted.

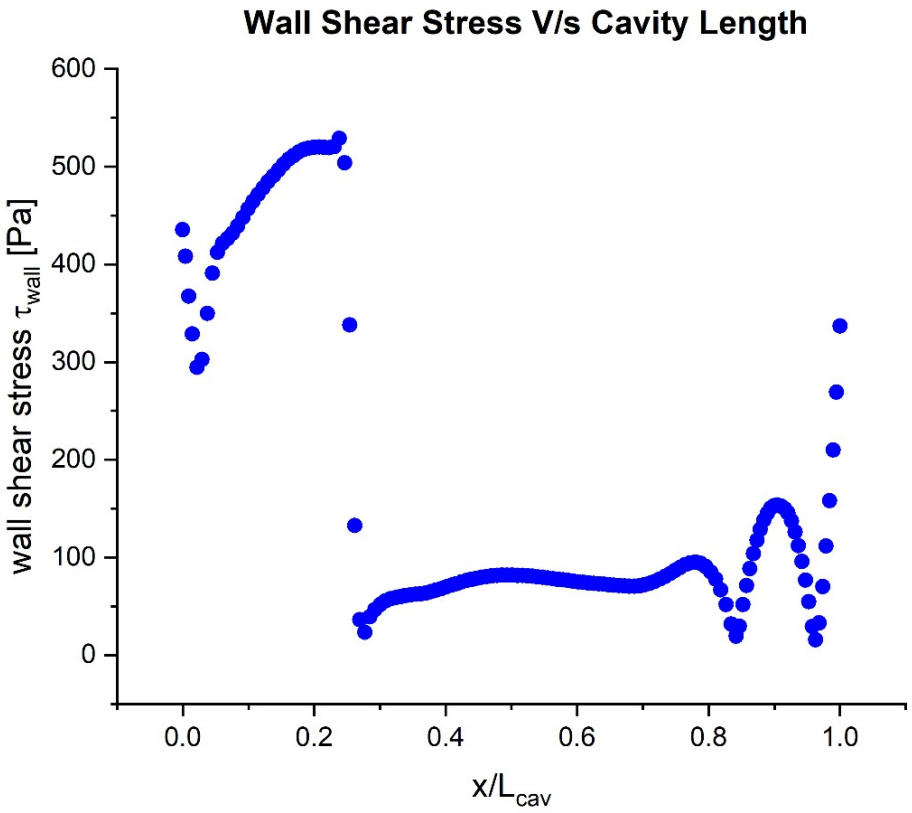

Figure 4.2: Wall shear stress of the lower wall of the cavity region of BDTN

4.2 Formula Used

Some parameters are used to evaluate the performance of the exhaust system. In normal flight mode, the thrust coefficient (C_t) and thrust vectoring angle δ are the most critical parameters. In SVTOL mode, lift coefficient (C_{fy}) is chosen to replace the thrust coefficient to evaluate the producing lift. The thrust vectoring angle is defined as:

$$\delta = atan(\frac{F_y}{F_x})$$

where F_x and F_y are the axial force, the x-component of force, and normal force or the y-component of force, respectively. They are obtained from the below equations:

$$F_x = \int_{A_2}(\rho v_x v_x + (P - P_b)).dA_x = \int_{A_{in}}(\rho v_x v_x + (P - P_b)).dA_x - F_{wall-x}$$

$$F_y = \int_{A_2}(\rho v_x v_y + (P - P_b)).dA_y = \int_{A_{in}}(\rho v_x v_y + (P - P_b)).dA_y - F_{wall-y}$$

where A_2 is the area of the nozzle at the second throat and A_{in} is the area of the nozzle inlet. v_x and v_y are the axial or the x-component of velocity and normal or the y-component of velocity, respectively. A_x is the projected area of the surface along the x-axis and A_y is the projected area of the surface along the y-axis. P_b is the ambient pressure while F_{wall-y} and F_{wall-x} is the total normal and axial component of resultant force along the geometry walls. Upon neglecting the projected area for SVTOL mode of flight the simplified equations then become:

$$F_y = F_{wall-y}$$

The thrust coefficient is then defined as the ratio of the resultant force or thrust to ideal isentropic thrust (F_{ideal}),

$$C_t = \frac{\sqrt{(F_x^2+F_y^2)}}{F_{ideal}}$$

The ideal force (F_{ideal}) can be obtained by the equation below:

$$F_{ideal} = \overline{m}_{in}\sqrt{(\frac{2\gamma}{(\gamma-1)}RT[1-(\frac{1}{NPR})^{(\frac{(\gamma-1)}{\gamma}}}$$

where γ is the specific heat ratio, R is the gas constant, and T is the total temperature at the inlet of nozzle in kelvin. NPR is the ratio of total pressure at the inlet of nozzle to the ambient pressure. For SVTOL the lift coefficient can be found from the equation:-

$$C_{fy} = \frac{F_y}{F_{ideal}}.$$

Using the formulas mentioned in this section, a detailed data analysis was performed to determine the flow behavior and thrust vector performance of the secondary conduit of the BDTN configuration.

4.3 Case Study A

. This case study was carried out for three different width ratios of the bypass conduit %, for varying mass flow rates or NPR. This was done with the aim to select the optimum flow conditions for the BDTN configuration meanwhile also achieving high performance. The bypass conduit width W_b, is a fundamental design parameter of the BDTN that directly influences the core mechanism of thrust vectoring and its associated performance metrics. A comprehensive study is included to investigate different conduit width to map the design space, identify optimal configurations that meet the specific STOL requirements of the military aircraft, and understand the trade-offs between thrust vectoring capability and overall engine performance. This section of the investigation also vaguely depicted the flow behavior for the closing and opening of the bypass conduit itself. The data from the computational post processing was further analyzed using the equations, mentioned in the section below, in EXCEL. The tables of the same are represented below.

NPR	$\overline{m}(Kg/s)$	$V(m/s)$	$F_{comp}(kN)$	$F_{ideal}(kN)$	$\delta°$	C_t	C_{fy}
1.50	6.19	204.67	1.27	1.58	7.08	0.80	0.10
3.00	13.64	323.45	4.41	5.47	10.10	0.80	0.14
4.00	18.12	334.64	6.06	8.04	19.74	0.75	0.25

Table 4.1: Flow behavior and performance data for $W_b = 3\%$

NPR	$\overline{m}(Kg/s)$	$V(m/s)$	$F_{comp}(kN)$	$F_{ideal}(kN)$	$\delta°$	C_t	C_{fy}
1.50	5.92	199.25	1.18	1.52	11.83	0.78	0.16
3.00	17.22	270.01	4.65	6.93	12.62	0.67	0.15
4.00	17.46	334.20	5.83	7.74	21.97	0.75	0.28

Table 4.2: Flow behavior and performance data for $W_b = 6.16\%$

NPR	$\overline{m}(Kg/s)$	$V(m/s)$	$F_{comp}(kN)$	$F_{ideal}(kN)$	$\delta°$	C_t	C_{fy}
1.50	5.84	192.27	1.12	1,499.13	12.31	0.75	0.16
3.00	12.98	321.62	4.18	5,231.49	19.91	0.80	0.27
4.00	21.30	302.15	6.44	9,456.49	12.00	0.68	0.14

Table 4.3: Flow behavior and performance data for $W_b = 9.57\%$

The graph is represented in three color format, green for $W_b/H_{in} = 3\%$, red for $W_b/H_{in} = 6.16\%$, and blue for $W_b/H_{in} = 9.57\%$, while the line style represents the performance parameters. The performance graph of thrust coefficient, represented by dotted line style indicates that at NPR 4 the maximum value achieved is 0.80, for W_b/H_{in} of 6.16%. While, the flow deflection, represented by solid line style, yielded

a maximum value of 22° at NPR 3 for the W_b/H_{in} of 3%. But at NPR 4 the thrust deflection δ attains a value of 21.5° can be observed in the figure. Thus, selecting the flow operating conditions at NPR 4 with the bypass conduit width ratio 6.16%.

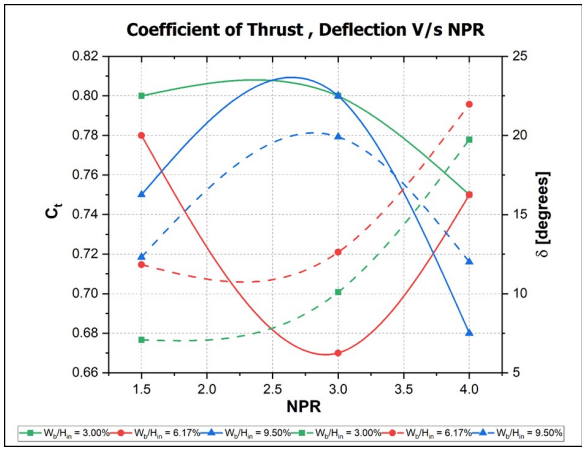

(a) C_t and δ vs NPR

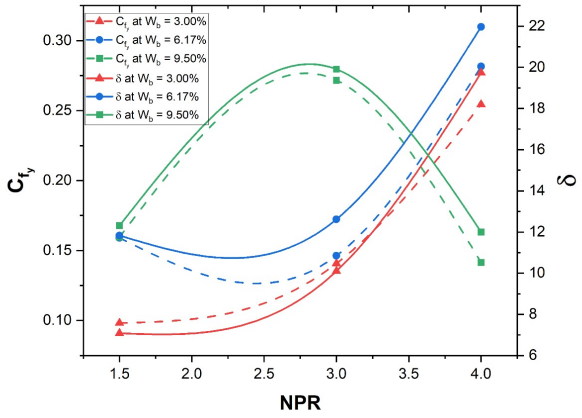

(b) C_{fy} and δ vs NPR

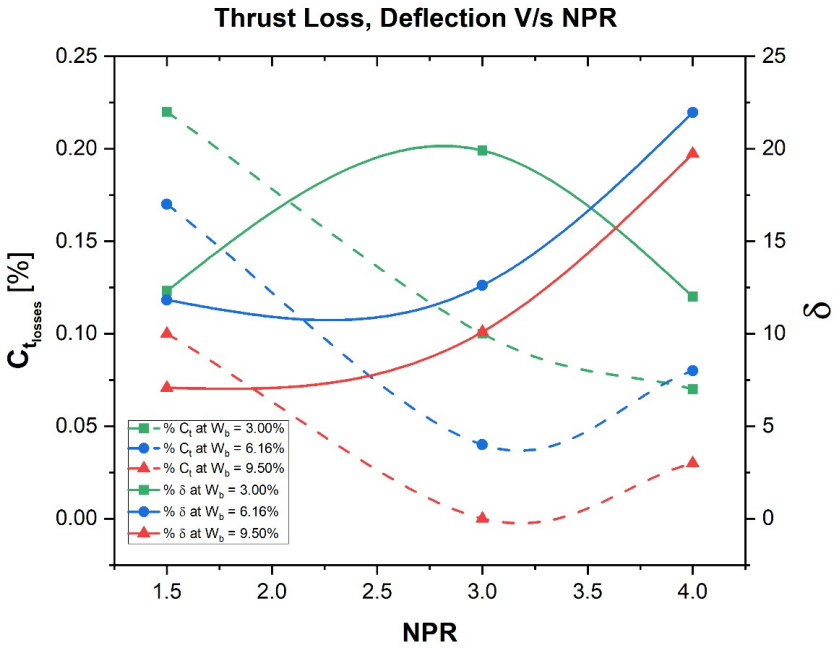

(c) Thrust loss and δ vs NPR

Figure 4.3: Performance graph of varying W_b % ratios for study 1

It can be assumed that the NPR 1.5 operating condition of the engine that represents the initial stage of of the flight mission profile that is ground roll. While the NPR 3 and 4 operating condition showcase the initial take-off or climb stage, hence can also be regarded as the STOL operating condition for the fighter jet engine. Upon selecting the flow operating condition of NPR 4 and duct geometry sizing of 6.16% of

H_{in}, for optimum STOL performance estimation for different injection angles α. The next case study includes the benchmark's computational velocity and mach contour range and the current investigation on the effect of the mentioned flow parameters on the proposed bypass design.

4.4 Case Study B

On selecting the flow engine STOL operating condition of NPR 4 with the duct geometry sizing of 6.16% , for the STOL performance estimation for different α of the BDTN configuration. This case study was conducted to investigate the performance of the BDTN exhaust flow performance for above mentioned STOL operating condition and determine the optimum α_{inj} for the proposed BDTN configuration. The graphical representation of the data from the simulation was plotted using Origin Pro software. The data table showing the thrust flow performance parameters is shown below.

Injection angle α°	**Deflection angle** δ°	**Thrust coefficient** C_t	**Thrust loss** $C_{t_{losses}}\%$	**Lift coefficient** C_{fy}
35	19.21	0.74	2.56	0.24
40	21.51	0.75	0.86	0.28
45	21.54	0.73	3.05	0.27
50	20.84	0.76	0.26	0.27
55	21.50	0.74	1.91	0.27
60	21.08	0.76	1.13	0.27
65	22.43	0.74	0.45	0.28
70	23.43	0.76	1.58	0.30
75	21.57	0.76	2.42	0.28

Table 4.4: Data of thrust flow performance for STOL operating condition

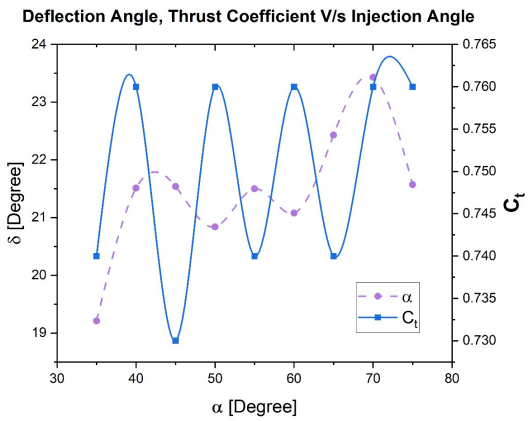

(a) δ and C_t vs α

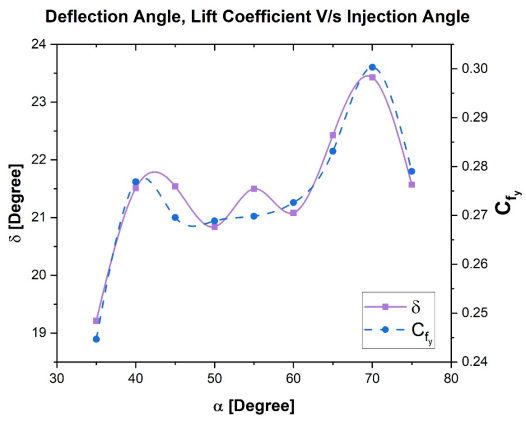

(b) δ and C_{fy} vs α

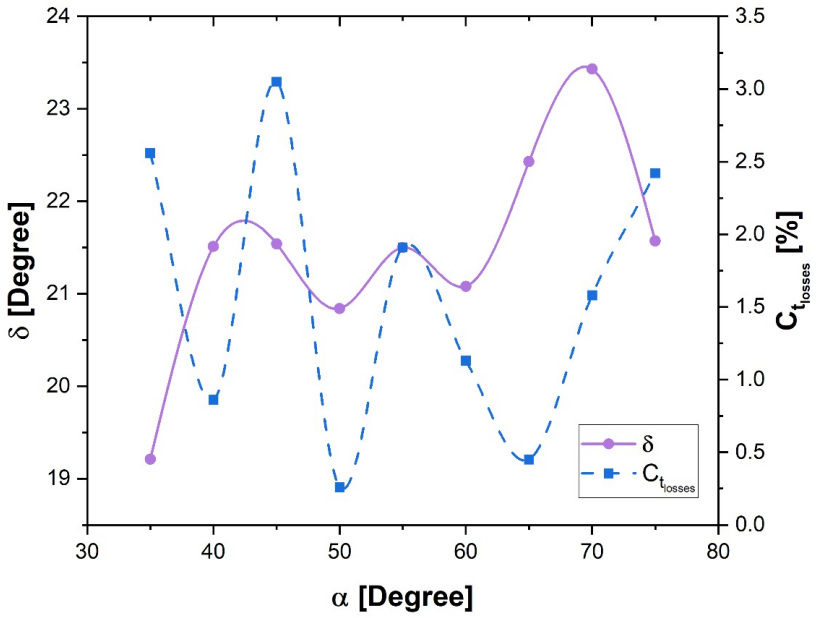

(c) δ and $C_{t_{loss}}\%$ vs α

Figure 4.4: Trend captured in the thrust vector performance parameters for STOL engine operating condition

The graphical representation of the data is shown in the figure above. It can be seen that for $\alpha = 70°$, the deflection achieved is around 24° with a maximum thrust coefficient C_t of 0.76 and minimal losses of around 1.6%. For the enhancement of aerodynamic lift, a lift coefficient(C_{fy}) of of 0.3 is observed to contribute in the maximum lift coefficient of the entire aircraft wing. The total lift generated by the aircraft during take off is the combination of the following:

- **Wing lift** ($C_{l_{wing}}$): It is the primary source of lift and is gernated by the airflow over the wing's airfoil at certain angle of attack, often enhanced by high-lift devices like flaps and slats. For STOL aircraft, the wing is typically designed to achieve a very high maximum lift coefficient at relatively low speeds.

- **Thrust vectoring lift (C_{fy}):** The downward component of the vectored thrust from the proposed BDTN exhaust configuration acts as an additional vertical force, effectively increasing the overall lift acting on the aircraft. This contribution allows the aircraft to take off at a lower airspeed than just relying solely on the wing lift.

For providing vertical force a thrust coefficient of 0.76 indicates that the efficiency of the design configuration in converting the engine's power into thrust. The crucial aspect of STOL is the thrust vector angle of 24°, which means a significant portion of the engine's thrust is being directed downward, providing a direct vertical force component. The mach contours for different injection angles capture the flow behavior phenomenons as shown below.

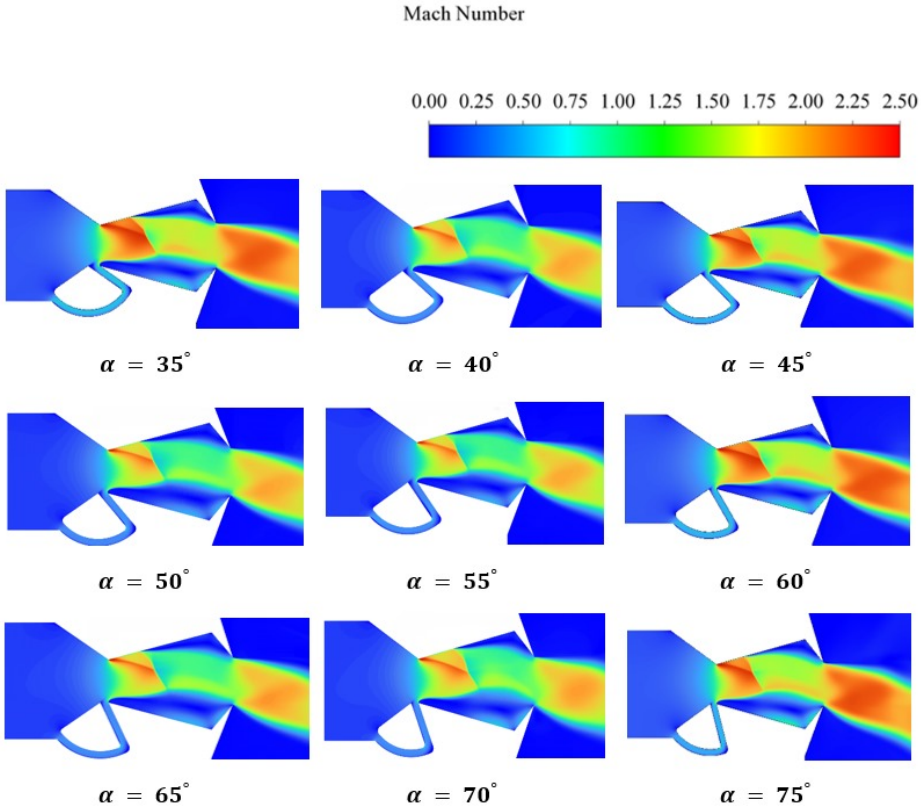

Figure 4.5: Exhaust flow M_a contours for NPR 4 with varying injection angle

This counteracts the aircraft's weight, reducing the airspeed required for the wings to generate enough aerodynamic lift for take-off. The efficiency consideration, shows relatively low thrust loss which suggests that the thrust vectoring is being achieved with reasonable efficiency, minimizing the penalty on forward thrust needed for acceleration. There is an important key observation to understand the flow phenomenon that results in a lower δ for the maximum thrust coefficient C_t achieved, i.e. 0.76, under the engine operating condition of NPR 4. This observation of two distinct $\delta$for similar C_t at two different α in a BDTN computational graph suggests a non-linear

relationship between the injection angle α and the resulting thrust vectoring and its impact on the thrust coefficient C_t. The potential reasons involved are listed below for the complex flow field dynamics within the exhaust.

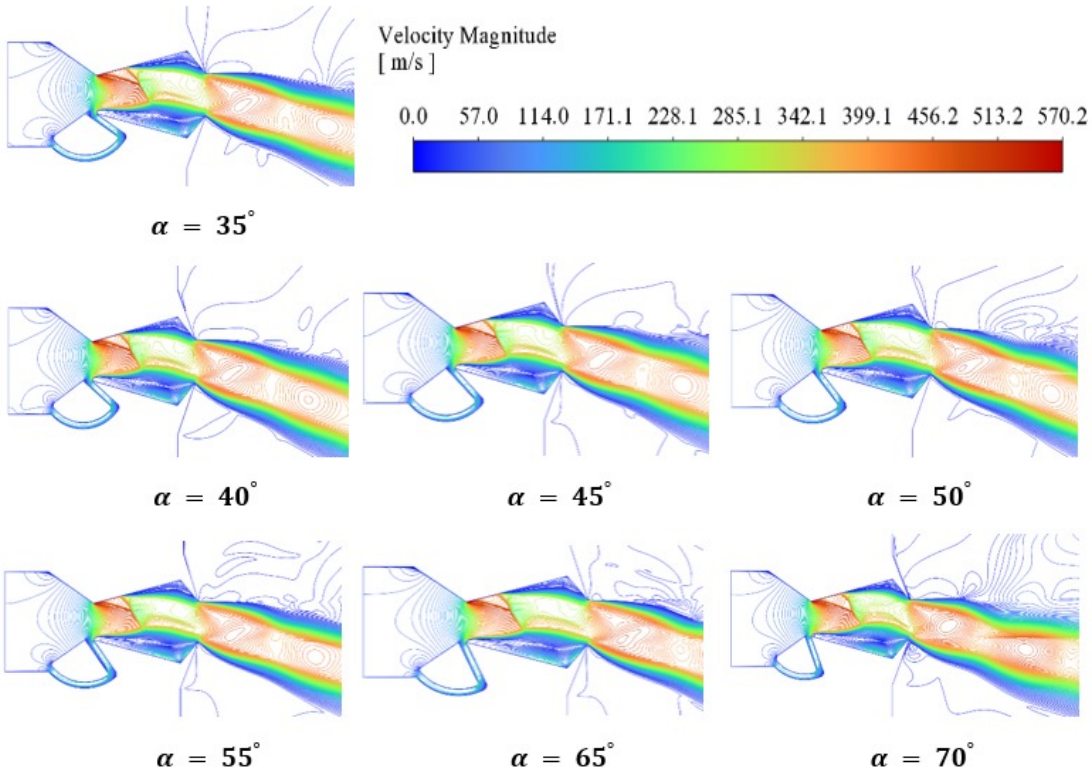

Figure 4.6: Exhaust flow velocity streamlines for varying α in BDTN configuration

- **Flow separation and reattachment:** The injection of a secondary flow at varying angles can trigger this phenomenon in the region of flow separation within the divergent section or the cavity of the BDTN configuration. These separation zones can significantly alter the pressure distribution along the nozzle walls, leading to different thrust vectoring angles and affecting the overall thrust coefficient.
- **Vortex formation and interaction:** The interaction of the primary and bypass flows can generate complex vortex structures within the BDTN exhaust configuration. The size, strength, and location of these vortices are highly sensitive to the injection angles. These angles might also promote the formation of dominant vortex structures that induce different levels of thrust deflection and associated losses.
- **Shock wave interactions:** In supersonic BDTN flows, the injected secondary flows can generate or modify shock wave patterns within the nozzle. The interaction of these shocks with the boundary layer and the primary flows can be

highly non-linear with respect to the injection angle, potentially leading to the observed discontinuity.

The above mentioned flow behavior can be captured in the streamline contours of the exhaust flow velocity, inside the BDTN configurations. Although, besides this another main culprit for the observed discontinuity could be due to geometric sensitivities like:

- **Bypass conduit and cavity geometry:** The specific geometry of the bypass duct , the cavity, and the contour of the main nozzle can significantly influence the interaction of the injected flow with the primary flow at varying α. This lead to amplified or dampened thrust vectoring effects and corresponding changes in the thrust coefficient, thus resulting in such phenomena in the data.
- **Injection port location and shape:** This can also play a crucial role. Different injection angles might result in the secondary flow interacting with the primary flow at different axial and radial locations, leading to varying degrees of momentum transfer and flow redirection, thus affecting the thrust coefficient differently.

To enhance the fidelity and accuracy of future investigations, the current reliance on RANS turbulence models should be superseded by higher-fidelity approaches such as LES or Detached eddy simulation (DES). This will offer a more nuanced representation of the complex turbulent flow structures inherent in BDTN operation. This involves particular concern in the intricate interaction between the primary and secondary flows and resulting thrust vectoring dynamics.

Chapter 5

Conclusion

The BDTN control is an upcoming advancement under fluid thrust vectoring technology for short vertical take off and landing operating conditions for the military jets. It is capable of achieving high performance as indicated from the numerical analysis conducted using ANSYS- CFD software in the previous section.

The computational results indicate a promising configuration for achieving short take-off and landing (STOL) for military aircraft, primarily through the generation of both direct thrust vectoring and enhanced aerodynamic lift. The optimized BDTN in the exhaust system configuration with the selected injection angle $\alpha_{inj} = 70°$ is considered to have the most efficient thrust vector performance where the thrust coefficient C_t of 0.76, lift coefficient C_{fy} of 0.3 and thrust vector angle δ of 24° with minimal thrust losses of around 1.6 %, at the STOL operating condition of the engine exhaust system of 4 NPR. The achieved C_{fy} represents the contribution from the proposed exhaust nozzle configuration in the maximum lift coefficient ($C_{l_{max}}$) of the entire aircraft wing.

In summary of the results, the proposed optimized BDTN configuration contributes to STOL by providing a significant vertical thrust component which acts as an additional lift force, that allows the aircraft to take off before reaching the conventionally required lift-off speed based solely on wing aerodynamics. The overall STOL performance will be a synergistic effect of the high maximum lift coefficient achievable by the aircraft's wing and the direct vertical force provided by the vectored thrust from the BDTN. The optimized 70° injection angle appears to be a sweet spot, balancing lift coefficient and thrust deflection with minimal performance losses. STOL is hence, achieved by enabling the aircraft to generate sufficient lift to become airborne at a significantly lower speed than conventional aircraft. This requires a high overall lift coefficient for the entire aircraft at a lower angle of attack and airspeed, which is contributed by the optimized BDTN exhaust system of the engine, through its direct thrust vectoring.

5.1 Future Scope

Furthermore, future computational research should incorporate a detailed analysis of the valve mechanism responsible for controlling the bypass flow. This includes parametrically studying various valve designs and their precise location within the bypass conduit The design is preferred for the military applications as it offers high thrust vectoring capabilities without the need of complex mechanical components, allowing for high maneuverable aircraft with excellent agility and control, especially in tight combat situations, all the while minimizing the weight and potential failure points by relying on the fluidic control to deflect the jet stream via bypass channels.

- **Advanced control systems integration:** Future research can focus on the seamless integration of BDTN with sophisticated digital flight control system. This will aim to optimize the aircraft's handling qualities and maximize the effectiveness of thrust vectoring during critical STOL phases.
- **Hybrid VTOL capabilities:** The core principles of thrust vectoring inherent in BDTN could be further explored to develop hybrid vertical take-off and landing (VTOL) aircraft. This would involve combining vectored thrust with other lift-generating mechanisms for enhanced versatility.
- **Multi-functional nozzle design:** Future iterations of BDTN could evolve into multifunctional exhaust systems. These advanced designs would aim to optimize performance not only for STOL but also for other crucial flight regimes, such as supersonic cruise efficiency and stealth characteristics, (e.g., reduced infrared signature).
- **Smart material and actuation:** The incorporation of smart materials and cutting-edge actuation systems in BDTN designs could lead to lighter, more responsive, and aerodynamically efficient thrust vectoring mechanisms.

The application of the BDTN include the enhanced operational flexibility, increases payload capacity, allow operation from smaller naval vessels, improved maneuverability and control capabilities of emergency landing. The design has a superior potential due to its high thrust vectoring angles, fluidic control, fast response time, lightweight design and reduced complexity. It has Stealth potential, which will limit the infrared to be restricted in the determination of external failure points for attack. The internal operation of the bypass channel has reduced noise generation unlike in the mechanical components. This design technology can be applied to various military aircraft like fighter jets, attack helicopters, unmanned aerial vehicles and missiles.

5.2 Domain Scope

While the primary focus has been on military STOL aircraft, the principles and technologies behind the BDTN could potentially find applications in other domains where controlled thrust vectoring or fluid flow manipulation is beneficial.

1. **Aviation**
    - *Noise reduction*: The controlled manipulation of the flow in BDTN offer avenues for reducing jet engine noise, particularly during takeoff and landing.
    - *Emergency control system*: A simplified BDTN can act as a backup control system in case of primary control surface failure.
2. **Spacecraft and Rocketry**
    - *Attitude control*: TV in vacuum is crucial as there is no aerodynamic effect on the exhaust flow and is simpler or more efficient in case of BDTN.
    - *Stage separation*: Controlled exhaust flow manipulation could potentially assist in cleaner or more controlled stage separation in multi-stage rockets.
    - *Landing or planetary bodies*: Without conventional runways, landing of spacecraft will require a controlled TV technique, offered by BDTN. It might also offer novel solutions for precise descent and landing on planetary bodies.
3. **Marine vehicles**
    - *Maneuvering and dynamic positioning*: TV in water jets or propellers make use of fluidic principles similar to BDTN, thus enhancing maneuverability of ships and submarines, particularly for dynamic positioning in challenging environments.
    - *Steering without rudders*: In smaller marine vessels, TV could potentially replace traditional rudder, simplifying the mechanical design.
4. **Industrial applications**
    - *Flow control in ducts and pipelines*: The principle of BDTN can bed adapted for controlling flow direction, mixing, or separation in industrial ducting and pipeline systems.
    - *Enhanced mixing in chemical processes*: Controlled jet impingement and flow manipulation using BDTN concept could improve mixing efficiency in chemical reactors or other industrial processes.

Appendices

Appendix A

Computation Methods

A.1 Governing Equations

A.1.1 Continuity Equation

The differential conservational form of continuity equation

$$\frac{\partial \rho}{\partial t} + \frac{\partial \rho u}{\partial x} + \frac{\partial \rho v}{\partial y} = 0$$

Integral Conservational Form of Continuity Equation

$$\frac{\partial}{\partial t} \iiint \rho dv + \iint \rho v ds = 0$$

A.1.2 Momentum Equation

Differential conservational form of Momentum Equation

$$\frac{\partial(\rho \vec{V})}{\partial t} + \nabla(\rho \vec{V} v) = \nabla P + F_{viscous} + \rho f_{body}$$

Differential Conservational Form of Momentum Equation in X direction

$$\frac{(\partial(\rho u))}{\partial t} + \frac{(\partial(\rho u u))}{\partial x} + \frac{(\partial(\rho u v))}{\partial y} = \frac{-\partial P}{\partial x} + \frac{(\partial \tau_{xx})}{\partial x} + \frac{(\partial \tau_{yx})}{\partial y} + \rho f_x$$

Differential Conservational Form of Momentum Equation in Y direction

$$\frac{(\partial(\rho v))}{\partial t} + \frac{(\partial(\rho v u))}{\partial x} + \frac{(\partial(\rho v v))}{\partial y} = \frac{-\partial P}{\partial y} + \frac{(\partial \tau_{xy})}{\partial x} + \frac{(\partial \tau_{yy})}{\partial y} + \rho f_y$$

A.1.3 Energy Equation

Differential Conservational Form of Energy Equation

Note: The Equation includes the expansion of the Heat Flux Terms and uses Stokes Postulates taken from "Fundamentals of Computational Fluid Dynamics" by John D Anderson

$$\frac{\partial}{\partial t} + \frac{\partial}{\partial x}[\rho(e + \frac{V^2}{2})u] + \frac{\partial}{\partial y}[\rho(e + \frac{V^2}{2})v] =$$
$$\rho q^{\cdot} - \frac{\partial Pu}{\partial x} - \frac{\partial Pv}{\partial y} + \frac{\partial}{\partial x}(K\frac{\partial T}{\partial x}) + \frac{\partial}{\partial y}(K\frac{\partial T}{\partial y}) + (\frac{\partial u\tau_{xx}}{\partial x}) + (\frac{\partial u\tau_{yx}}{\partial y}) + (\frac{\partial v\tau_{xy}}{\partial x}) + (\frac{\partial v\tau_{yy}}{\partial y})$$

Methods	**Significance**
SIMPLE (Semi-Implicit Method for Pressure-Linked Equations)	· Suitable for steady-state, incompressible, and mildly compressible flows. Uses a pressure-correction approach to couple pressure and velocity.Can be less accurate for high-speed compressible flows.
SIMPLEC (SIMPLE with Collocated)	· An extension of the SIMPLE scheme, using a collocated grid approach. · Suitable for steady-state, incompressible, and mildly compressible flows. · Offers improved accuracy and stability compared to SIMPLE.
COUPLED (Coupled Solver)	· Solves the momentum and continuity equations simultaneously. · Suitable for steady-state and transient, compressible and incompressible flows. · Offers improved accuracy and robustness, especially for high-speed compressible flows.
PISO (Pressure-Implicit with Splitting of Operators)	· Suitable for transient, compressible, and incompressible flows.
PIMPLE (Pressure-Implicit with Splitting of Operators and Modified Link)	· A combination of PISO and SIMPLEC, suitable for transient, compressible, and incompressible flows.

Table A.1: Computational Model and Numerical Setup

The methodology is designed for the objective, focusing on the optimization of the nozzle design using the computational tool ANSYS-FLUENT as mentioned above. The table below shows computational methods used in ANSYS-Fluent CFD For nozzle, COUPLE method is preferred in ANSYS CFD analysis, especially for subsonic operations. Hence, the same will be considered in the performance estimation of the

BDTN Geometry.

A.2 Turbulence $k-\epsilon$ Model

This turbulence model consists of transport equations, i.e. turbulent kinetic energy (k) and rate of the turbulent dissipation (ϵ). The governing equations are:

$$\frac{\partial(pUik)}{\partial xi} + \frac{\partial(pk)}{\partial t} = \frac{\partial}{\partial(xj)}[\mu + \frac{\mu t}{\sigma}\frac{\partial k}{\partial xj}] + S_k + G_k + Y_M + G_b - p\epsilon....(1)$$

$$\frac{\partial(p\epsilon)}{\partial t} + \frac{\partial(pUi\epsilon)}{\partial xi} = \frac{\partial}{\partial xj}[\mu + \frac{\mu t}{\sigma}\frac{\partial \epsilon}{\partial xj}] + [C_1\epsilon\frac{\epsilon}{k}(Gk + C_3\epsilon G_b) - (\frac{2p\epsilon^2}{k}) + S\epsilon]....(2)$$

Turbulence Model	**k-ϵ**	**k-ω**	**SST-ω**
Advantages	Improves Accuracy in Prediction flows with strong streamline curvature and vortices	Have better performance for the region adjacent to the wall and captures boundary layer separation.	It includes the advantages of both the models k-ω and k-ϵ , It automatically switches between the equations according to the requirement.
Disadvantages	Fails to capture the near wall turbulent boundary layer.	Usually encounters sensitivity issues in free-stream region leading to inaccurate results.	It is computationally more time consuming and highly sensitive.

Table A.2: Comparison of Methods used in ANSYS and their significance

The preferred turbulence model for this project is k-ϵ as it focuses on improving the accuracy in predicting the free flow. Since the project does not involves any study regarding the boundary wall, so k-epsilon has been used instead of above two mentioned for the ease of simulation.

A.2.1 Model Setup

The Viscous realizable K-ϵ model with 2 equations was used with standard parameters.

Model Parameters	Values
c-2 ϵ	1.9
TKE Prandtl Number	1
TDR Prandtl Number	1.2
Energy Prandtl number	0.85

Table A.3: Domain computational model parameters

A.2.2 Sutherland law

The 2D compressible RANS equations are used to solve the numerical method. Roe's flux difference splitting scheme and second order upwind scheme are adopted to discretize the inviscid and viscous flux terms on control volume surfaces in RANS equations. The dynamic viscosity in governing equations is computed by the Sutherland law =, the equation of which is stated below

$$\mu = \mu_o[(\frac{T}{T_o})]^{1.5}\frac{T_o+S}{T+S}$$

Where: T is static temperature, T_o is the reference temperature, and μ_o is the reference viscosity value at reference temperature. S id an effective temperature, called the Sutherland constant. For air $\mu_o = 1.716 \times 10^{-5}$ kg/m.s, at $T_o = 273.11K$, and S = 110.56 K

A.2.3 Realizable $k-\epsilon$ Model

This is chosen as the turbulence model, solving the turbulent viscosity μ_t with two modeled transport equations for k and ϵ. The same are listed below:

$$\frac{\partial(\rho k)}{\partial t} + \frac{\partial(\rho k u_j)}{(\partial x_j)} = (\frac{\partial}{\partial x_j})[(\mu + \frac{\mu_t}{\sigma_k})(\frac{\partial k}{\partial x_j})] + G_k + G_b - \rho\epsilon - Y_m + S_k$$

$$(\frac{\partial \rho\epsilon}{\partial t}) + (\frac{\partial \rho\epsilon u_j}{\partial x_i}) = \frac{\partial}{\partial x_j}[(\mu + \frac{\mu_t}{\sigma_\epsilon})\frac{\partial \epsilon}{\partial x_j}] + \rho S\epsilon C_1 - \rho C_2 \frac{\epsilon^2}{(k+\sqrt{\epsilon})} + C_{1\epsilon}\frac{\epsilon}{k}C_{3\epsilon}G_b + S_\epsilon$$

Where, $C_1 = max[0.43, \frac{\eta}{(\eta+5)}]$, $\eta = S\frac{k}{\epsilon}$, $S = \sqrt{S_{ij}S_{ij}}$, $C_{1\epsilon}$ and $C_{3\epsilon}$ are constant variables. To close the momentum equations, Boussinesq approach is used to model the Reynold's stresses terms. Boussinesq hypothesis and eddy viscosity definition which are given below:

$$(-\rho\overline{(u_i'u_j')} = \mu_t((\frac{\partial u_i}{\partial x_j}) + (\frac{\partial u_j}{\partial x_i})) - \frac{2}{3}(\rho k + \mu_t(\frac{\partial u_k}{\partial x_k}))\delta_{ij},$$

$$\mu_t = \rho C_\mu \frac{k^2}{\epsilon}.$$

In realizable k-ϵ model, C_μ is not a constant anymore, and is a function of the mean strain and rotation rates, which are given below respectively,

$$C_\mu = \frac{1}{(A_o + A_s \frac{kU^*}{\epsilon})},$$

$$U^* = \sqrt{(S_{ij}S_{ij} + \tilde{\Omega_{ij}}\Omega_{ij})},$$

$$\tilde{\Omega_{ij}} = \Omega_{ij} - 2\epsilon_{ijk}\omega_k,$$

$$\Omega_{ij} = \overline{\Omega_{ij}} - \epsilon_{ijk}\omega_k,$$

where $\overline{\Omega_{ij}}$ shows the rate of rotation tensor viewed in a moving reference frame with angular velocity ω_k. The constant $A_o = 4.04$, A_s calculation is shown below:

$$A_s = \sqrt{6cos(\phi)},$$

where

$$\phi = \frac{1}{3}cos^{-1}(\sqrt{6W})$$

$$W = \frac{S_{ij}S_{jk}S_{ki}}{\tilde{S}^3},$$

$$\tilde{S} = \sqrt{S_{ij}S_{ij}},$$

$$S_{ij} = \frac{1}{2}(\frac{\partial u_i}{\partial x_j} + \frac{\partial u_j}{\partial x_i}).$$

References

1. The big Lockheed Martin F-35 Lightning II topic
2. Lightening F 35 B II engine nozzle technique model
3. F-35B 1/4 Scale engine layout | 3D CAD Model Library | GrabCAD
4. Defense Visual Information Distribution Service- https://www.dvidshub.net/2010-2020
5. Meet the US Navy's new $13 billion aircraft carrier - CNET - The USS Gerald R. Ford (CVN 78) is the most technologically advanced warship ever built.**Fox Van Allen**Dec. 10, 2019 11:28 a.m. PT
6. Smith, J.(1986). Rolls-Royce Pegasus: The Development Story. Rolls-Royce Heritage Trust. (Provides historical context on swivel nozzle in the Harrier).
7. Ningjun LIU, Zhihao CAI, Yingxun WANG, Jiang ZHAO, Fast level-flight to hover mode transition and altitude control in tiltrotor's landing operation, Chinese Journal of Aeronautics,Volume 34, Issue 1,2021,ISSN 1000-9361,
8. Gutmark, E., Wygnanski, I., and Papamoschou, D. (The dynamics of coherent structures in turbulent jets. Physics of Fluids A: Fluid Dynamics, 1(11), 1781-1785. (While focused on jet dynamics, it provides fundamental understanding relevant to SGI).
9. Reba, R. (2004). Counterflow jet control for thrust vectoring. Journal of Aircraft, 41(4), 759-767. (Discusses the principles and performance of counter-flow injection).
10. Younes, Khaled and Hickey, Jean-Pierre. (2020). Fluidic Thrust Shock-Vectoring Control: A Sensitivity Analysis. AIAA Journal. 58. 1-4. 10.2514/1.J058922.
11. Wu , Kexin and Kim, Tae Ho and Kim, Heuy. (2021). Visualization and analysis on the thrust vectoring control in three-dimensional dual-throat nozzles. Journal of Visualization. 24. 10.1007/s12650-020-00734-y.
12. Ruifeng Pan, Jinglei Xu, Yuqi Zhang, Yao Li, Shuai Huang, Numerical simulation and experiment of a bypass dual throat nozzle with tab modification, Aerospace Science and Technology, Volume 144, 2024, 108816, ISSN 1270-9638.

13. J. C. Páscoa, A. Dumas, M. Trancossi, P. Stewart, and D. Vucinic, “A review of thrust-vectoring in support of a V/STOL non-moving mechanical propulsion system,” 2013, *Springer-Verlag Wien*. doi: 10.2478/s13531-013-0114-9.

14. Afridi, Saadia, Tariq Amin Khan, Syed Irtiza Ali Shah, Taimur Ali Shams, Khawar Mohiuddin, and David John Kukulka. 2023. "Techniques of Fluidic Thrust Vectoring in Jet Engine Nozzles: A Review" Energies 16, no. 15: 5721. https://doi.org/10.3390/en16155721.

15. Curran, E.T.; Cousineau, R.J. Fluidic thrust vectoring using counterflow. AIAA J. 1996, 34, 2089-2095.

16. Donahue, C.J.; Thyson, J.S.; Platzer, M.F. Experimental investigation of fluidic thrust vectoring with a rectangular nozzle. J. Aircr. 2005, 42, 148-154.

17. F. Capone, P. Smereczniak, D. Spetnagel, and E. Thayer, “Comparative investigation of multiplane thrust vectoring nozzles,” in *AIAA/ASME/SAE/ASEE 28th Joint Propulsion Conference and Exhibit, 1992*, American Institute of Aeronautics and Astronautics Inc, AIAA, 1992. doi: 10.2514/6.1992-3263.

18. Fujihira, K. (2025) “Systematic method for identifying unsuitable land for development: biodiversity, disaster risk, and topography,” Academia Environmental Sciences and Sustainability. Academia.edu Journals, 2(2). doi: 10.20935/AcadEnvSci7647.

19. Y. Zhang, J. Xu, R. Pan, Y. Li, Z. Ma, and S. Huang, “Numerical investigation of short takeoff and landing exhaust system using bypass dual throat nozzle,” *Aerosp Sci Technol*, vol. 138, Jul. 2023, doi: 10.1016/j.ast.2023.108316.

20. S. Huang, J. Xu, K. Yu, Y. Wang, and R. Pan, “Design and experimental study of a bypass dual throat nozzle with the ability of short/vertical takeoff and landing,” *Aerosp Sci Technol*, vol. 121, Feb. 2022, doi: 10.1016/j.ast.2021.107301.

21. K. Hakim, H. Toufik, and Y. Mouloudj, “Study and Simulation of the Thrust Vectoring in Supersonic Nozzles,” *Journal of Advanced Research in Fluid Mechanics and Thermal Sciences*, vol. 93, no. 1, pp. 13–24, 2022, doi: 10.37934/arfmts.93.1.1324.

22. Afridi, S.; Khan, T.A.; Shah, S.I.A.; Shams, T.A.; Mohiuddin, K.; Kukulka, D.J. Fluidic Thrust Vectoring in Jet Engine Nozzles. Encyclopedia. Available online: https://encyclopedia.pub/entry/47854.

23. Afridi, S.; Khan, T.A. Numerical investigation of fluidic thrust vectoring using secondary flow injection in a dual throat nozzle. Proc. Inst. Mech. Eng. Part G J. Aerosp. Eng. 2021, 235, 3600-3610.

24. Afridi, S.; Khan, T.A. Multi-objective nozzle design optimization for maximum thrust vectoring performance. Proc. Inst. Mech. Eng. Part G J. Aerosp. Eng. 2022, 237, 587-599.

25. Hamedi-Estakhrsar, M.; Ferlauto, M.; Mahdavy-Moghaddam, H. Numerical study of secondary mass flow modulation in a Bypass Dual-Throat Nozzle. Proc. Inst. Mech. Eng. Part G J. Aerosp. Eng. 2020, 235, 488-500.

26. Wang, Y.; Xu, J.; Huang, S.; Lin, Y.; Jiang, J. Computational study of axisymmetric divergent bypass dual throat nozzle. Aerosp. Sci. Technol. 2019, 86, 177-190

27. Wang, Y.; Xu, J.; Huang, S.; Jiang, J.; Pan, R. Design and Preliminary Analysis of the Variable Axisymmetric Divergent Bypass Dual Throat Nozzle. J. Fluids Eng. 2020, 142, 061204.

28. B. BERRIER and R. RE, "A review of thrust-vectoring schemes for fighter applications," American Institute of Aeronautics and Astronautics (AIAA), Jul. 1978. doi: 10.2514/6.1978-1023.

29. F. Capone, P. Smereczniak, D. Spetnagel, and E. Thayer, "Comparative investigation of multiplane thrust vectoring nozzles," in *AIAA/ASME/SAE/ASEE 28th Joint Propulsion Conference and Exhibit, 1992*, American Institute of Aeronautics and Astronautics Inc, AIAA, 1992. doi: 10.2514/6.1992-3263.

30. Afridi, S.; Khan, T.A.; Shah, S.I.A.; Shams, T.A.; Mehmood, K.; Li, W.; Kukulka, D. Numerical Investigation on the Thrust Vectoring Performance of Bypass Dual Throat Nozzle. Energies 2023, 16, 594.

31. "AIAA Student Design Competition Homeland Defense Interceptor: Gavial Virginia Polytechnic Institute," 2006.

32. Ugwueze, Osita, Thomas Statheros, Nadjim Horri, Michael A. Bromfield, and Jules Simo. 2023. "An Efficient and Robust Sizing Method for eVTOL Aircraft Configurations in Conceptual Design" *Aerospace* 10, no. 3: 311. https://doi.org/10.3390/aerospace10030311.

33. **Targeting a Specific y+ Value for your Turbulent Flow CFD Simulation – 2019 – Simtech Engineering**

34. Mesh quality : july 30th 2024 : SimScale

35. Turbulance Models in CFD: Ideal Simulations

36. Courant Number : Ideal SImulations